Pulsed Laser Ablation in Liquid (PLAL) for nano-particle generation

Brian Freeland[1,2], Eanna McCarthy[1], Sithara Sreenilayam[1], Greg Foley[2], Dermot Brabazon[1]

[1]I-Form, Advanced Manufacturing Research Centre, & Advanced Processing Technology Research Centre, School of Mechanical & Manufacturing Engineering, Dublin City University, Collins Avenue, Dublin 9, Ireland

[2]School of Biotechnology, Dublin City University, Collins Avenue, Dublin 9, Ireland

Abstract

Nanoparticles, broadly spherical pieces of material with diameters in the nanoscale range, have a number of advantageous physical, chemical, electrical, and optical properties. These unique properties make them suitable for a wide range of applications including sensing, medical therapeutics, printed electronics, and anti-fouling/anti-microbial surfaces. Pulsed laser ablation in liquid (PLAL), also known as laser ablation synthesis in solution (LASIS), is an attractive, green method for producing ligand-free nanoparticles in solution. These nanoparticles can be produced from a wide range of target materials and avoids the use of hazardous, environmentally-unfriendly chemicals. In this chapter, the key applications, conventional generation methods of nanoparticles, as well as the background and cutting edge of PLAL are reviewed.

1. Introduction

Nanomaterials are defined as objects with one or more lengths in the nanoscale in the range of 1 - 100 nm [1]. Nanomaterials may have a single nanoscale dimension (thin films or sheets), two nanoscale dimensions (nanowires or nanotubes), or three nanoscale dimensions (nanoparticles). Within the dimension range of 1-100 nm, nanoparticles can range from small clusters of atoms to larger particles [1].

The unique chemical and biological functionality, high surface areas, and electrical, mechanical, and optical properties of nanomaterials make them highly suited to a number of applications such as sensing [1–3], separation [4], energy storage [5], display technology [6], printable circuits [7], and drug delivery [8]. Nanomaterials have high surface-to-volume

ratios, making them well-suited to many sensing applications [1–3]. For example, in a fully 1-dimensional single-walled carbon nanotube (CNT), every atom is at the surface giving it an ideal surface-to-volume ratio [2]. The relationship between the percentage of atoms at or near the surface with the size of a nanoparticle is exponentially decreasing with a particle diameter of 5 nm containing 60% volume fraction within 0.5 nm of the surface, a particle diameter of 20 nm containing 12% volume fraction within 0.5 nm of the surface and a particle diameter of 100 nm presenting just 6 % volume fraction within 0.5 nm of the surface [1].

Nanomaterials also have attractive electronic properties. When dimensions are greater than the mean free path of a carrier within the material, a nanoscale object will have the same electron transport properties as the bulk material. However, when one or more of the dimensions are smaller than this, the electronic properties become dependent on the dimension(s) [9]. This allows electronic properties, such as voltage outputs, turn on/off currents, and characteristic sensor responses, to be tuned by control of the nanoscale dimensions [10–12]. The optical properties may also be varied with control of the shape and dimensions. Dreaden et al. presented the different photon absorption behaviour (due to collective conduction electron excitation or plasmon resonance) with different sizes and shapes of nanomaterials, identifiable by the differing visual colours [13].

Pulsed laser ablation in liquid (PLAL), also known as laser ablation synthesis in solution (LASIS), is a method of nanomaterial fabrication where a pulsed laser is focused on a solid target in a liquid medium, ablating the material to form nanomaterials in solution [14]. This method allows for production of nanoparticles using various target materials, without the need for environmentally hazardous solvents. However, commercially-viable mass production with this method has been limited by batch-based production leading to low outputs.

In this chapter, the key applications of nanoparticles will be reviewed, a general overview of nanoparticle generation and a more detailed review of PLAL nanoparticle generation will be presented, including the current state-of-art for PLAL and issues facing commercialisation of the process.

2. Nanoparticle applications

2.1 Sensing

The high surface areas, and optical and electrical properties of nanoparticles make them ideal for sensing applications. Most nanoparticle-based sensors can be broken down into colorimetric, fluorescence, or electrochemical sensors [15]. The photon absorption behaviour, and thus the visual colour, of nanoparticles is strongly dependant on the size and shape of the particles [13]. These colourful light-scattering properties allow nanoparticles to be used similarly to fluorescent dyes. The light-scattering power of a single nanoparticle label is stronger than a single fluorescent label, and the light signals are not subject to photobleaching and require less complex instrumentation [16].

Typically, colorimetric sensing uses larger nanoparticles (>30 nm) which exhibit strong visible light-scattering. Gold nanoparticles are particularly popular, as they have a surface plasmon resonance, where conduction electrons near the surface of the metal are stimulated into oscillation by an external electromagnetic wave, with a maximum absorption at a resonance frequency. For nanoparticles, the wavelength of this resonance is strongly dependant on the size, shape, aggregation, and medium refractive index [17]. Changing these parameters will change the visual colour of the nanoparticles. For example, well-dispersed gold nanoparticles with sizes of 10-50 nm will appear red, while aggregation of the particles will change the colour to blue [18–20]. This provides a mechanism for colorimetric sensing.

A typical aggregation based sensing process was detailed in a work by Chen et al., describing colorimetric detection of melamine in milk using gold nanoparticles [21]. Melamine is an industrial compound used in manufacturing that can be used to adulterate milk to create false high protein values. Excessive melamine intake is harmful, especially to infants and adolescents, driving the need for reliable methods of detecting melamine in milk [22]. The gold nanoparticles were chemically synthesised by a trisodium citrate reduction, then chemically modified to asymmetrically graft polyethylene glycol (PEG) as a stabiliser. The presence of melamine in the milk disturbs the electrostatic balance on the surface of the nanoparticles, promoting the formation of aggregates, shown in Figure 1. This results in a colour shift, as described above, which can be detected by eye or with spectrophotometry. The authors found this method to be sensitive and reliable. Methods may also be based on "anti-aggregation", where the target prevents or impedes aggregation of the nanoparticles [15]. An example of an anti-aggregation method is presented by Ramezani et al., in a work

where gold nanoparticles were used in colorimetric sensing of tetracycline [23]. Tetracyclines are broad-spectrum antibiotics used in veterinary medicine. Residues of tetracyclines in food products could have undesirable side-effects on human consumers, creating a need for tetracycline sensing. Gold nanoparticles were chemically synthesised by a citrate reduction and combined with a triple helix molecular switch (THMS) made up of a purchased aptamer and signal transduction probe (STP). THMS is stable in the absence of tetracycline allowing ambient salt (NaCl) in the medium (serum or milk in this study) to trigger aggregation of the nanoparticles, leading to a colour change to blue [23]. When the targeted tetracycline is present, the aptamer in the THMS binds to the target, and the released STP binds to the nanoparticles inhibiting aggregation leaving the red colour. As with aggregation-based methods, the colour can be identified visually or with spectrophotometry.

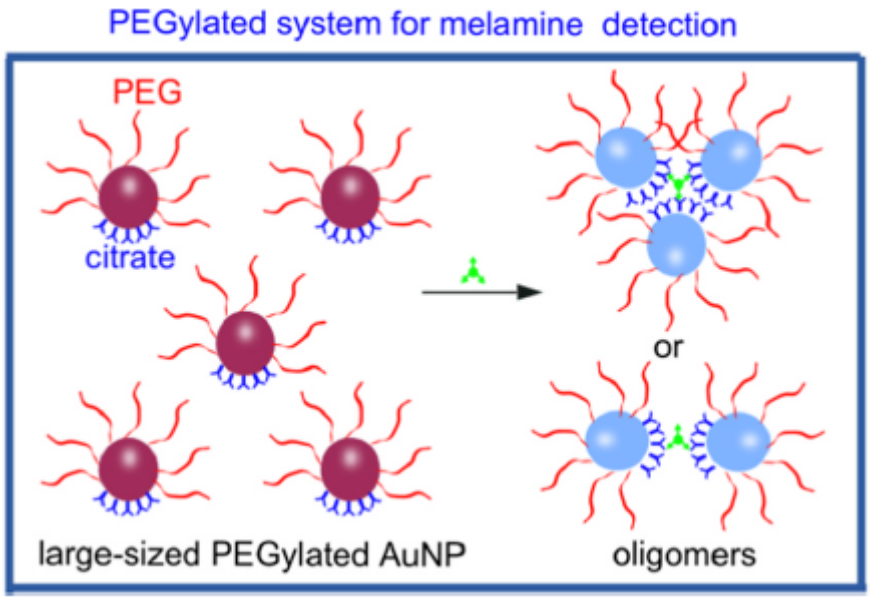

Figure 1: Principle of asymmetrically PEG-modified gold nanoparticle aggregation based colorimetric sensor for detection of melamine (Reproduced from [21]).

Fluorescence sensing is based on the use of organic or inorganic fluorophore dyes, which suffer from some limitations. The dyes can have low absorption coefficients and weak signals, limiting sensitivity and response, are prone to photobleaching, leading to short lifetimes, and are potentially toxic [16,24]. Fluorescent nanoparticles, made up of organic fluorophores encapsulated in a particle matrix, are much bright than single dye molecules, and are more stable and biocompatible than un-encapsulated fluorophores [24]. Nanoparticles

can also be used a quenchers in fluorescence resonance energy transfer (FRET) based sensing [25]. FRET is a highly distant dependant, non-radiative process where an excited donor fluorophore transfers energy to an acceptor [15,25]. The initiation of FRET can act to quench or turn-off fluorescence, as energy that would be otherwise radiatively released through fluorescence is transferred into the acceptor, which can act as a sensing method [15]. For example, Xu et al. describe the use of gold nanoparticles in a FRET based sensing strategy for sensing the neurotransmitter dopamine [25]. In this work, a dopamine binding aptamer and a fluorescent (rhodamine B) were used with citrate-synthesised gold nanoparticles. When dopamine is not present, the aptamer attaches to the gold nanoparticles, preventing NaCl induced aggregation, and FRET quenching can take place between the nanoparticles and the fluorophores. When dopamine is present, the aptamer will preferentially attach to the target dopamine, allowing the nanoparticles to cluster, preventing FRET quenching. A schematic of this can be seen in Figure 22 [25]. The authors found the method to be rapid, simple, selective, and sensitive.

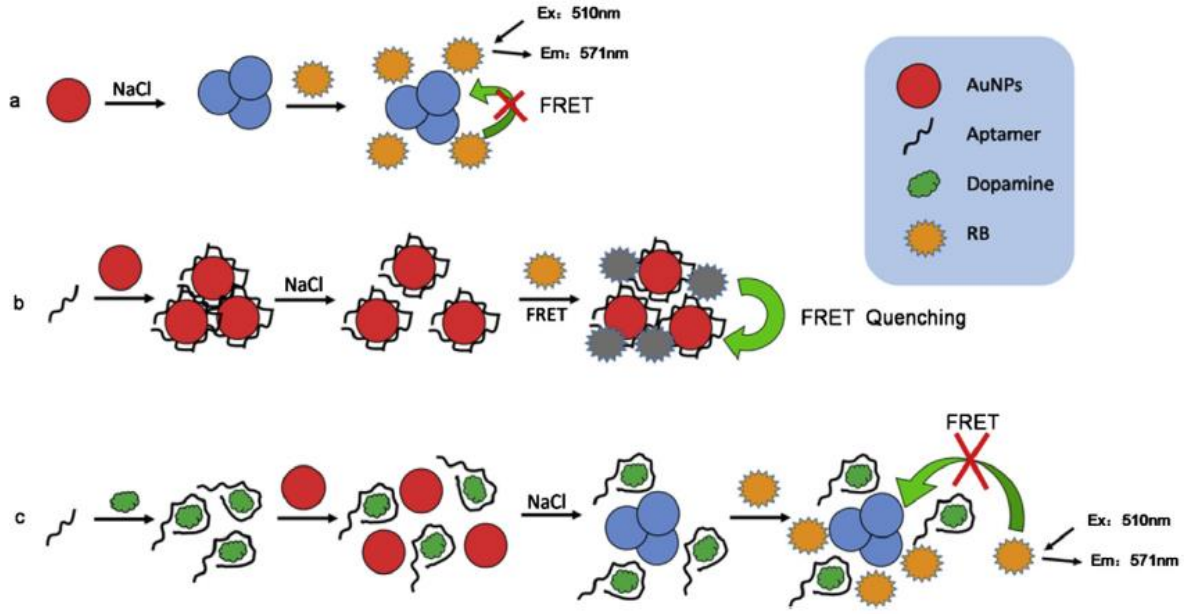

Figure 2: Schematic illustrating FRET quenching based dopamine sensing using gold nanoparticles (AuNPs) and rhodamine B (RB) (Reproduced from [25]).

In electrochemical sensing, nanoparticles are often used to modify sensing electrodes to achieve the desired sensitivity and selectivity [15]. Electrochemical sensors work by the variation of the electric response of a device due to chemical interactions between target analytes and the surface of the electrode [26,27]. A general schematic for an operating

electrochemical biosensor is presented in Figure 33 [28]. The high surface-to-volume ratio of nanoparticles offers a large sensing surface, and they also offer excellent electrical conductivity and biocompatibility [29]. An example of nanoparticle use in electrochemical sensing can be seen in a work by Raj et al., where immobilised gold nanoparticle arrays were used for voltammetric sensing of dopamine [30]. The authors note that detection of dopamine is inhibited by the presence of interfering compounds in biological samples, and as such ensuring good selectivity in sensing electrodes is a major goal. Treatment or coating of electrodes is one way to achieve this. The authors applied an amine terminated self-assembled monolayer (cystamine) to a gold electrode, then immobilised chemically synthesised gold nanoparticles on the surface. The nanoparticle coated electrode was shown to be able to distinguish between dopamine and a typical interfering compound (ascorbate), which was not possible with the bare gold electrode, with good sensitivity, selectivity, and anti-fouling.

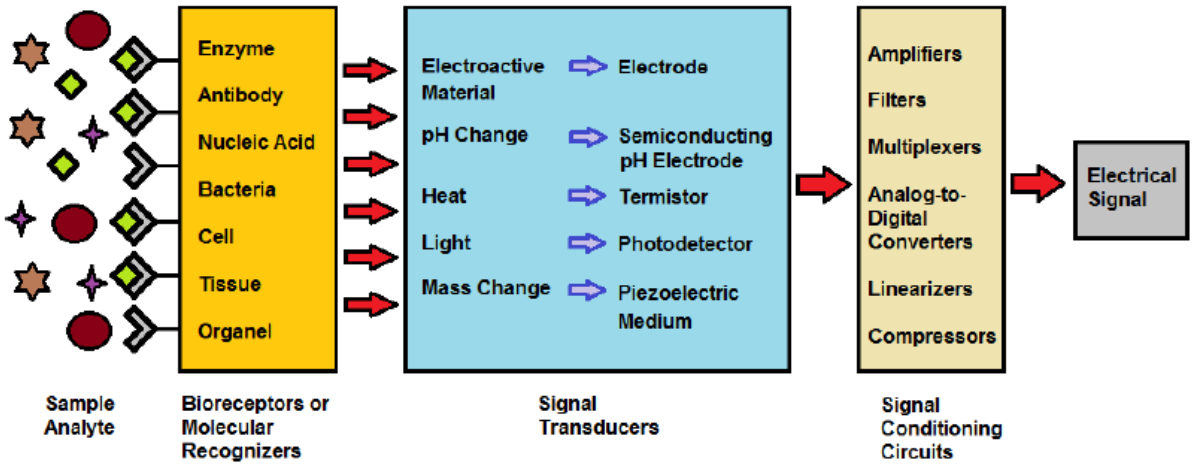

Figure 3: Schematic of the main subsystems of an operating biosensor (Reproduced from [28]).

2.2 Conductive Inks

Deposition or printing of conductive inks is an efficient method for the production of conductive coatings and circuits [31]. Printed electronics can be low cost, light weight, optically transparent, and used in flexible electronics [32]. Conductive patterns can be printed to flexible substrates such as paper [33–35] or polymer [36,37]. Flexible electronics are of interest for radio frequency identification (RFID) tags [33,35], robotics [38,39], and

biomedical applications [40,41]. Conductive inks of conductive nanomaterials in solution are commonly used, such as silver nanowires [42], silver nanoparticles [36,43], copper nanoparticles [44], and carbon nanotubes [45]. Silver nanoparticle inks are one of the most commonly used, due to their high conductivity, and low oxidisation [46,47]. Silver nanoparticle inks are typically in aqueous or solvent media, stabilised with surfactants or polymers, and then dried and/or sintered after printing [46]. An example of silver nanoparticles being used in a conductive ink can be seen in a work by Matyas et al. [36]. In this work, silver nanoparticles were produced by a solvothermal precipitation synthesis method using silver nitrate salt, an organic precipitation agent, and a polymer stabilising agent. The ink was prepared by dispersing the nanoparticles in deionised water with ultrasonication, with 0.1 ml of dispersion stabiliser added per 10 ml of dispersion fluid. The final viscosity of the ink ranged from 8 to 12 cPs. The ink was then ink-jet printed at 35 °C onto a PET-based PCB substrate at 45 °C. After printing, the substrate and printed circuit were dried in a vacuum oven at 120 °C for 20 min to sinter the nanoparticles. An SEM image of the printed silver nanoparticle layer can be seen in Figure4 [36]. With this method, a working flexible antenna was successfully created.

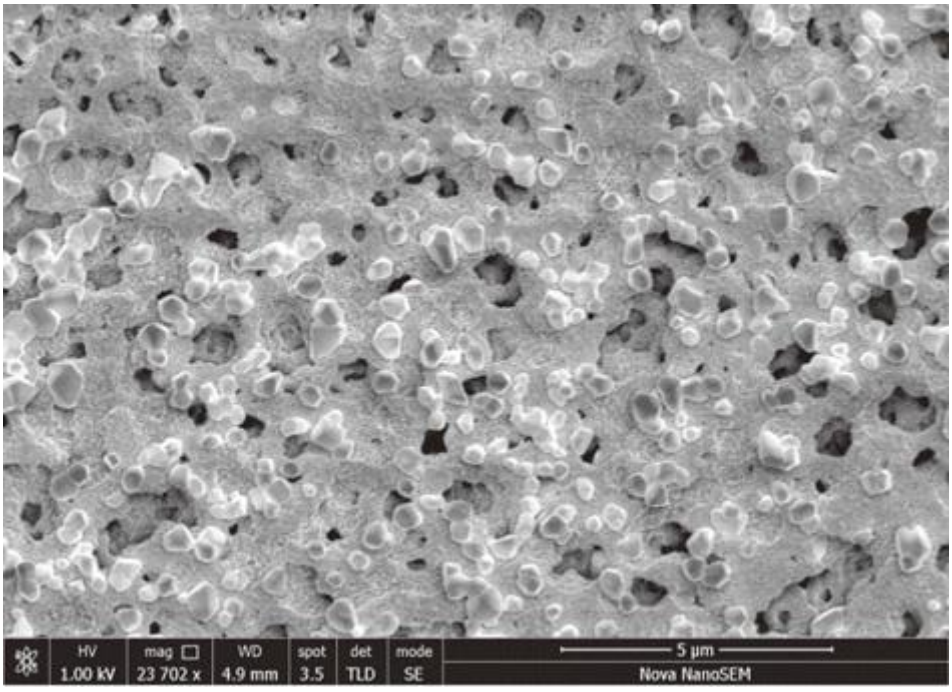

Figure 4: SEM image of a printed silver nanoparticle circuit on a PET substrate (Reproduced from [36]).

2.3 Anti-fouling

Fouling is the deposition or accumulation of unwanted material on the surface of a solid. This gathering of material can inhibit the mechanical, chemical, or electrical function of devices, lead to contamination, or, in the case of medical tools or devices, lead to infection. Fouling is a significant problem for applications like sensing electrodes [48] and osmosis membranes [49]. Anti-fouling surfaces, with properties such as superhydrophobicity, self-cleaning, and drag reduction, which resist fouling are therefore highly desirable [50].

Silver and its compounds are well known for their antimicrobial, biocidal effects [51–53]. Silver nanoparticles are particularly popular for use in antimicrobial coatings due to the high surface area, allowing for more reactive surface-oriented groups compared with the bulk material [52]. Silver nanoparticles have a number of mechanisms against micro-organisms: particles attaching to the cell surfaces, disrupting the function of the cell wall [54,55]; permeating the cell and damaging the DNA, proteins, or other cell constituents [55,56]; and releasing reactive silver ions [55,57]. Titanium dioxide nanoparticles also have good anti-fouling properties and wettability [58]. A work by Nguyen et al. describes the use of silver nanoparticles and titanium dioxide nanoparticles for antifouling effects on a forward osmosis membrane [49]. The build-up of deposits of organic matter on osmosis membranes can reduce their permeability and shorten their lifetime. The authors note that silver the antibacterial effect of silver nanoparticles can be lost if the particles become covered by a biofilm. In this work silver nanoparticles were combined with titanium dioxide, which is known for its propensity to decompose organic matter, to create an improved anti-fouling surface. Silver and titanium oxide nanoparticles were deposited in separate wet chemical processes onto the porous surface of commercial forward osmosis membranes, which were tested for their anti-fouling behaviour. They found the modified membrane had excellent antibacterial effect, almost 11 times less bacterial growth compared to the as-received membrane, and that the flux reduction due to fouling was lessened for the modified membrane due to the delayed onset of fouling.

2.4 Therapeutics

Nanoparticles have been used in therapeutics for illnesses such as Alzheimer's [59–61], cancer [62–64], and atherosclerosis [65]. Nanoparticles may be used in imaging based therapeutic techniques [63], drug delivery [59], or gene delivery [66]. Chemical synthesis is a common method of producing nanoparticles, however the chemicals involved in their

production may be hazardous to human health, and as such alternative production methods may be more attractive for therapeutic applications [63].

The unique optical properties and the surface plasmon resonance of gold nanoparticles make them of interest for imaging-based therapeutic techniques or photo-thermal therapy [63]. Photo-thermal therapy is a cancer therapy where photon energy is converted into heat energy to destroy cancer cells [67]. Synthetic molecules which absorb the applied photons more strongly than the surrounding tissue can be applied to a tumour to localise the heating. In plasmonic photo-thermal therapy (PPTT), gold nanoparticles are introduced to the cancerous cells by intravenous or intratumoural injection, and then exposed to light [67,68]. The light, typically near infra-red, causes oscilliation of the free electrons in the gold nanoparticles due to surface plasmon resonance, and this oscillation energy can be emitted as heat through nonradiative decay. This strong localised heating then destroys the cancer cells [67].

Nanoparticles can also be a drug delivery method [59–61,64]. As carriers or vessels for drugs, nanoparticles have the potential advantages of penetration of biological barriers like cell membranes or the blood brain barrier, protection of the drug from premature chemical or physical breakdown, and surface modification to help with solubility and delivery or limit toxicity [59,64,69,70]. Improving the specificity/targeting of drugs is also possible [59,63].

Chemotherapy drugs, for treatment of cancer, are traditionally delivered orally or intravenously, causing them to affect the entire body [63]. The resulting negative side effects drive an interest in targeted or localised drug delivery methods. Nanoparticles are one method of achieving this. Chemotherapy drugs can be loaded or attached to nanoparticles. Tumour tissue tends to have leaky vasculature, which will cause an accumulation of intravenously applied nanoparticles from the blood stream as a form of "passive" targeting [63]. However the strength of this targeting varies with the type of tumour due to variation in the vasculature [71]. In "active" targeting, ligands of tumour specific biomarkers are conjugated to the nanoparticle carrier. The ligand's interaction with the tumour causes the nanoparticles to be internalised by the tumour cells by endocytosis [71]. Careful selection of the ligand is necessary, but greater targeting can be achieved for a greater range of tumours using active compared to passive targeting. Gold nanoparticles are well-suited to this application due to their biocompatibility, non-toxic nature, and tuneable sizes, geometries, and properties [72,73]. For example, Chen et al. describe the conjugation of a chemotherapy agent methotrexate to gold nanoparticles to treat tumours [74]. The gold nanoparticles were chemically synthesised with a citrate-reduction. A colloidal solution of the nanoparticles was

then mixed with methotrexate and a sodium phosphate buffer. The mixture was centrifuged and rinsed, and then redispersed in the buffer. A diagram of the conjugation can be seen in Figure 55 [74]. A coordinate-covalent bond attaches the methotrexate molecule to the gold nanoparticle. The authors observed that the drug accumulates at a faster rate, to a higher amount, when conjugated to the gold nanoparticles compared to the drug alone being administered.

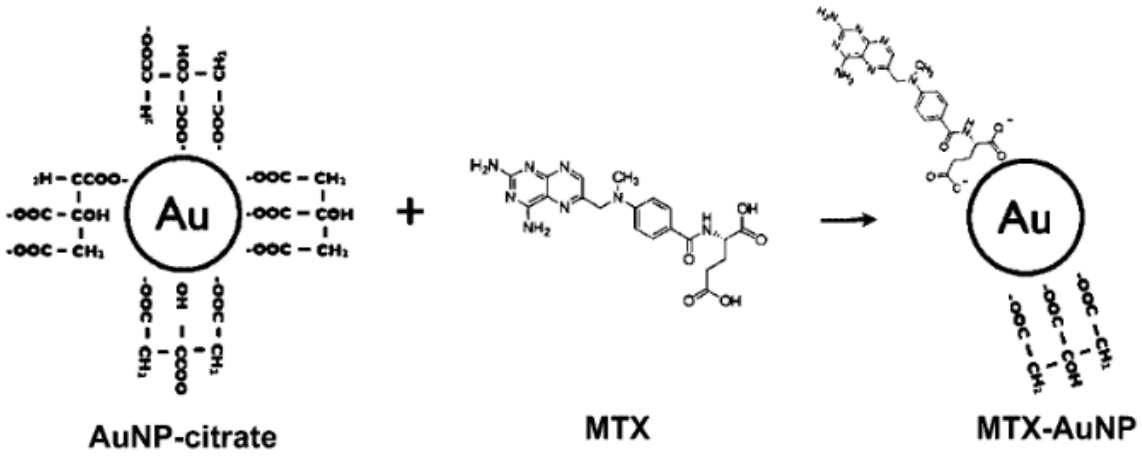

Figure 5: Schematic of the conjugation of methotrexate (MTX) to the citrate-reduced gold nanoparticles (AuNP) (Reproduced from [74]).

Diseases like Alzheimer's disease (AD) which affect the brain and central nervous system can be difficult to treat, due to the blood brain barrier [59]. Drugs used in AD therapy, typically orally administered, tend to have side effects due to a lack of selectivity for the therapeutic targets [60,61]. This issue can be mitigated with drug carriers capable of crossing the blood brain barrier, allowing sufficient amounts of the drug to be delivered to the brain and central nervous system at lower overall doses, minimising off-target effects [59]. Nanoparticle drug carriers can successfully deliver drugs through the blood brain barrier [75]. The nanoparticles used are typically dendrimers (dendritically branched molecules), polymer nanoparticles, and lipid nanoparticles [59,75].

3. Non-Laser based Nanoparticle Generation

3.1 Chemical Generation

Chemical synthesis is one of the most common methods of producing metal nanoparticles [76]. Reduction based methods in solution are typical for metallic and alloy nanoparticles [77]. Silver nanoparticles are most commonly produced by chemical reduction with organic or inorganic reducing agents, such as sodium citrate, ascorbate, sodium borohydride, elemental hydrogen, polyol process, Tollens reagent, N-dimethylformamide (DMF), and poly (ethylene glycol)-block copolymers [78]. The reducing agents reduce Ag^+ leading to the formation of metallic silver, which agglomerates into nanoparticles. Stabilising agents can be used to prevent further agglomeration of the nanoparticles into larger clusters [79]. The particles may also be functionalised. Similar chemical reduction methods are used for gold nanoparticles, using reducing agents such as borohydrides, aminoboranes, hydrazine, formaldehyde, hydroxylamine, saturated and unsaturated alcohols, citric and oxalic acids, polyols, sugars, hydrogen peroxide, sulfites, carbon monoxide, hydrogen, acetylene, and monoelectronic reducing agents [80]. As with silver, stabilising agents are added to maintain dispersion of the particles. Citrate-based reduction methods are most common for gold. Citrate can act as both a reducing and a stabilising agent for gold nanoparticles. This method is known as the Turkevich method, developed by Turkevich et al. in 1951 [81], and then improved upon by Frens in 1973 [82]. In this method chloroauric acid ($HAuCl_4$) is boiled and trisodium citrate is then added under stirring [80]. Citrate can also be used solely as a stabilising agent, with a separate reducing agent [83].

A disadvantage of some chemical synthesis methods are their use of chemicals and solvents (such as hydrazine and sodium borohydride) which may be hazardous to humans or the environment [63,84]. An interest in "green" - ecologically safe - methods of generating nanoparticles has driven some movement away from chemical synthesis to other methods such as PLAL, but also in developing green synthesis methods using biological agents in the reducing process [84]. These methods are generally based on reducing metal salt solutions with a biological agent, and have been used with silver, gold, platinum, mercury, selenium, palladium, and others, including alloys and metal oxides [84–86]. A general diagram for the process, for silver nanoparticles, can be seen in Figure [84]. Biological agents may be taken from plants, microbial, algal, and cyanobacterial sources, and typically the agents chosen act as both reducing and stabilising agents [84]. For example, Dwivedi and Gopal report on the production of silver and gold nanoparticles using an extract from Chenopodium album leaves [87]. Chenopodium album is a weed that is found in Asia, North America, and Europe. The authors prepared a leaf extract by boiling fresh, washed leaves in distilled water. The

extract was then used as a reducing agent to produced silver and gold nanoparticles from silver nitrate and auric acid, respectively, in aqueous solution. The reaction was carried out at room temperature for 15 min. This simple, convenient, green method successfully produced 10-30 nm nanoparticles for both silver and gold.

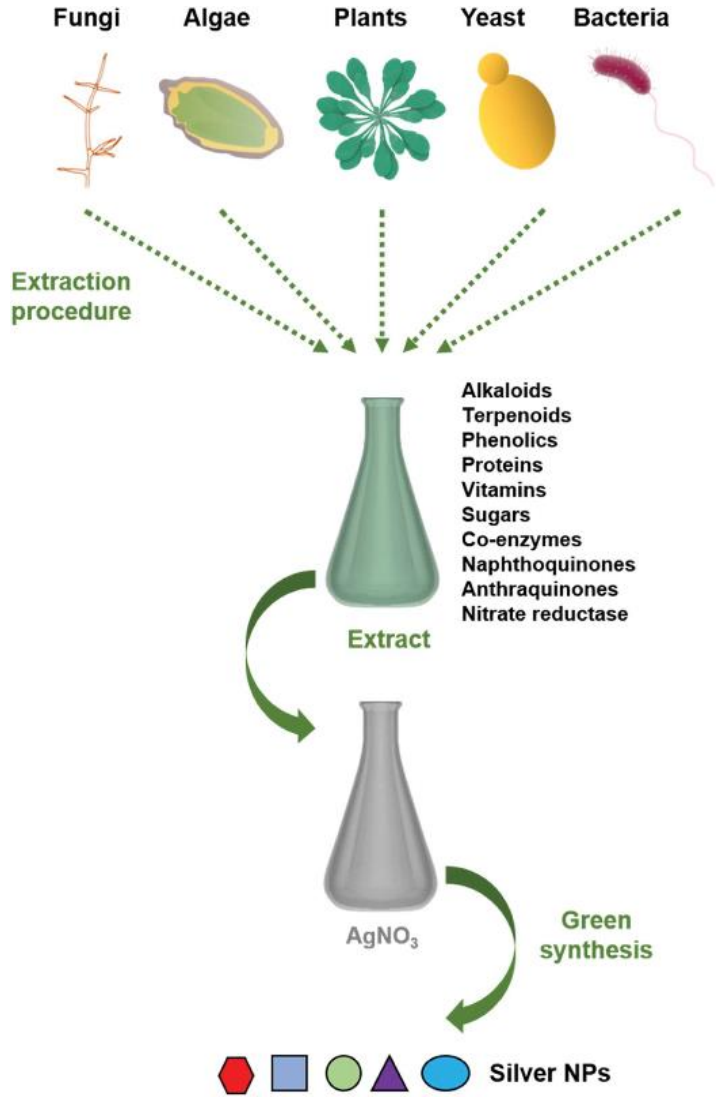

Figure 6: Schematic for green synthesis of silver nanoparticles using various biological agents (Reproduced from [84]).

3.2 Physical Generation

Methods of nanoparticle generation based on physical processes can avoid the use of potentially hazardous or contaminating chemicals and solvents, and can achieve more uniform distribution of nanoparticles compared to chemical processes, however they may require higher capital costs for equipment, and higher energy consumption, for thermal or

laser based processes [78]. Evaporation-condensation methods, where a source material is evaporated by heating, for example in a tube furnace, and condensed into nanoparticles are one physical generation method. Magnusson et al. report on the production of gold nanoparticles by evaporation with a tube furnace, aerosolisation, size selection, and thermal reshaping [88]. In this method, the source material is placed in a ceramic boat in a tube furnace, heated to create a high pressure vapour which is then carried by a nitrogen carrier gas flowed through the furnace, creating the aerosolised particles. The particles are size selected in a differential mobility analyser (DMA), which relies on the particles being charged beforehand. The selected particles are then reheated in a second furnace to allow reshaping of the particles, and then size selected again by a second DMA. With this method, the authors were able to produce gold nanoparticles in the 20 nm size range, with near spherical shape and near single crystallinity.

Arc discharge has also been used for physical nanoparticle generation. Lo et al. describe the use of arc discharge to produce silver nanoparticle suspensions [89]. A diagram of the experimental setup is presented in Figure 7 [89]. A silver bar submerged in a dielectric liquid is used as the electrode. An electric arc is generated, heating the metal to 6,000-12,000 °C. The evaporated material quickly cools in the surrounding low temperature dielectric liquid and forms silver nanoparticles dispersed in this cooling medium. The authors report the novel process was, with the correct processing parameters, successful in producing well dispersed nanoparticles in deionised water with average sizes ranging 6-25 nm, and avoiding aggregation. Lung et al. describe the use of arc discharge to produce gold nanoparticles [90]. Gold wires submerged in deionised water were used as both the positive and negative electrodes. Arc discharge between the wires, as with the process described by Lo et al. [89], evaporates the metal, which cools and condenses in the surrounding deionised water. The authors report the method is cheap, rapid, environmentally friendly, and successfully produces gold nanoparticles, without the need for any surfactants or stabilisers.

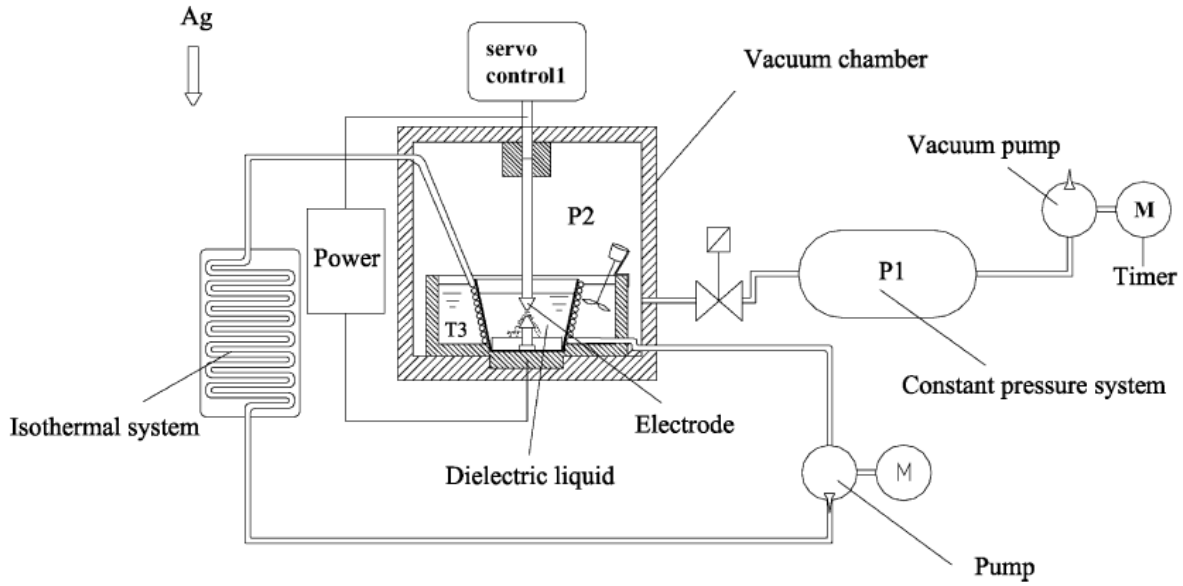

Figure 7: Schematic diagram of the arc discharge process for silver nanoparticle generation (Reproduced from [89]).

Nanoparticles can also be produced with physical grinding or milling. Grinding methods can be divided into dry or wet grinding [91–93]. Production of nanoparticles by dry ball milling presents a simple, low cost, environmentally friendly, high yield method [91,93]. Arbain et al. report on the production of iron oxide nanoparticles by dry milling [93]. In this work a planetary ball mill was used under atmospheric conditions with steel grinding media in a 3:1 ratio with the raw material, which was high purity hematite (Fe_2O_3) powder. Nanoparticles were successfully produced with a minimum size of 76.6 nm, without the need for any chemical additives, however there was some aggregation of the particles.

Wet milling allows the production of suspensions, and can produce more stable nanoparticles with the use of stabilising agents, however this reduces the simplicity of the method, and may add cost and reduce the environmentally friendliness. Knieke et al. report the production of tin oxide and aluminium oxide nanoparticles by wet grinding [94]. Aluminium oxide powder of average particle size 2 µm or tin oxide powder of average particle size 1.6 µm were used, in deionised water and denatured ethanol, with a zirconia grinding medium. The powders were premixed with the wet chemicals in a stirred vessel, pumped through a heat exchanger into the mill, and returned to the stirred vessel [94].

Gold and silver nanoparticles have also been produced by wet grinding. Pimpang et al. report on manual grinding of silver and gold nanoparticles [92]. Silver powder and gold foil were used as raw materials, with deionised water and ethylene glycol and 5 wt% polyvinyl alcohol as medium and stabilisers. The nanoparticles were produced by hand grinding in an agate mortar. The authors successfully produced gold and silver nanoparticles with optical properties indicating particle sizes of 140-150 nm.

Grinding/milling may be used as part of a chemical production process to shape or stabilise the nanoparticles. Balaz et al. report on a combined chemical-physical production method for silver nanoparticles, by wet milling using a plant-based reducing agent [95]. Silver nitrate and polyvinylpyrrolidone were used with an extract from *Origanum vulagare* L. plants. The leaves, flowers, and stems of *Origanum vulgare* L., a herb in the mint family, were dried and powdered to fine particles, which were then added by 10 g to 100 mL of distilled water. The mixture was then heated to 60 °C for 10 minutes, cooled down, and filtered to produce the reducing agent. The nanoparticles were produced in solution by chemical reduction with the reducing agent, then processed in a stirring media mill with a zirconium dioxide milling medium. The stabilising agent, polyvinylpyrrolidone, was added in this milling process. This method successfully produced stable silver nanoparticle suspensions, with two size groups of average size 7 nm and 38 nm, respectively.

4. Laser based Nanoparticle Generation

4.1 Pulsed Laser Ablation in Liquid (PLAL) Generation

Pulsed Laser Ablation in Liquid (PLAL) is a physical method of nanoparticle generation where a pulsed laser is focused on a solid target in a liquid medium, to ablate material from the target, creating nanoparticles in solution [14]. The laser light irradiating the solid target is partial absorbed by the target (with the remaining light being scattered or transmitted). The energy is absorbed by the excitation of bound electrons in the target. If the absorbed energy is high enough, the bound electrons will be released, ionising the material. These free electrons can continue to absorb the laser light by inverse Bremsstrahlung, leading to further heating and ionisation [96]. The result of this is the formation of high pressure plasma, which expands out from the target in a plume, initially with high speeds which generates a shockwave through the liquid. As the plume expands it forms a gas cavitation bubble in the liquid, which collapses under the surrounding pressure, producing another shockwave which

expels the material into the liquid, cooling and condensing them into solid form, producing nanomaterials such as nanoparticle colloids. A diagram for this process is shown in Figure 8 [97]. The collapse of the bubble may produce a rebound which then collapses, potentially producing another rebound, and so on, giving behaviour similar to a damped oscillator [98–100].

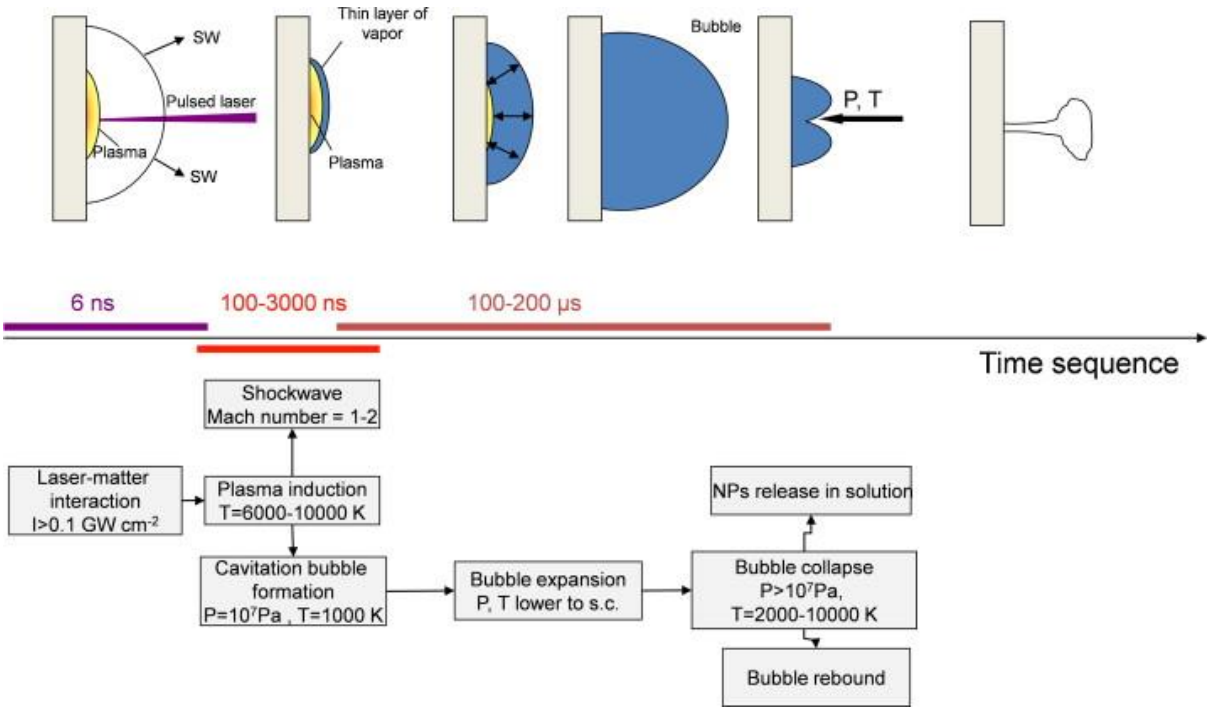

Figure 81: The time sequence of the processes involved in pulsed laser ablation in liquid (Reproduced from [97]).

The morphology of the nanomaterials produced can be controlled by altering the process parameters such as laser fluence, wavelength, and ablation medium. The PLAL process is highly adaptable, capable of producing a variety of nanomaterials (nanoparticles, nanocubes, nanorods, etc.) with a variety of compositions (metals, alloys, oxides, carbides, hydroxides, etc.) [101]. The method generally doesn't require additional chemical agents, beyond the liquid solvent medium, making the method eco-friendly and producing surfactant and ligand free nanoparticles. Some applications, like catalysis and biomedicine, require ligand free nanoparticles, that would otherwise need to be obtained through cleaning of the nanoparticles [102].

There has been some investigation into the cavitation bubble and nanomaterial formation process in PLAL. Ibrahimkutty et al. monitored the formation of nanoparticles in the cavitation bubble using high time resolution, small angle x-ray scattering [103].

Nanoparticles were produced by PLAL of a gold ribbon target in water by an Nd:YAG laser (1064 nm, 6 ns, 10 mJ, 200 Hz) focused to a 100 µm diameter spot size. The gold ribbon was continuously in motion perpendicular to the laser, to present a fresh ablation site for each pulse, with a flow of deionised water in the same direction to transport the nanoparticles away from the beam focus. The cSAXS 13.6 keV beamline at the Swiss Light Source was used as the x-ray source. The x-rays are transmitted through the cavitation bubble, where some of the photons will be scattered by the forming nanoparticles, to a detector [103].

The authors report detection of two species within the ablation region: small particles of 8-10 nm, and larger, agglomerated, particles of ~45 nm diameter. Such bimodal size distributions are commonly reported for PLAL nanoparticles [104–107]. The authors report that the presence of primary particles decays towards the top of the bubble, with some primary particles found outside of the bubble perimeter prior to its collapse [103]. They note that initial plasma velocities for laser plasma plumes created in vacuum have been found to be 10^8 mm/s, which is sufficient to allow injection of atomic species from the cavitation bubble into the surrounding liquid [108,109]. Larger particles have already formed, possibly due to collisions between the primary particles in the plume/bubble. These particles are not detected close to the target, which the authors attribute to the probability of agglomeration over time and height, and the confinement and cooling of particles nearer the vapour-liquid interface.

Shih et al. investigated the bimodal distribution which commonly occurs in PLAL by experiment and modelling [110]. Atomistic modelling of picosecond laser ablation of silver in water was carried out, and imaging of cavitation bubbles in PLAL experiments, to examine the mechanics behind the formation of the bimodal size distribution. Their model suggests the formation of a transient hot molten metal layer at the interface with the surrounding liquid which plays a critical role in the nanoparticle formation process. The liquid in contact the hot molten layer becomes supercritical creating a metal-water mixing region which is a precursor to the cavitation bubble. The conditions in this relatively low-density mixing region are conducive to the formation of small nanoparticles from the evaporating metal (<10 nm). The authors note a secondary formation process, where the molten layer itself may break up under the pressure exerted by the surrounding supercritical liquid, forming larger nanoparticles (10-20 nm) without evaporation. This suggests a bimodal distribution, even in the absence of agglomeration. The model indicates ejection of this material from the mixing region into the surrounding, cooler, liquid, which was confirmed by the imaging experiments. The authors note good agreement between the model, the imaging results, and the resulting nanoparticles

(analysed by centrifuge and transverse electron microscopy), supporting the conclusion that these two formation mechanisms lead to the bimodal particle size distributions commonly observed for PLAL.

De Giacomo et al. investigated the dynamics of PLAL cavitation bubbles during nanoparticle production using three complementary optical techniques: optical emission spectroscopy (OES) to characterise the plasma, fast shadowgraphs to for the plasma and cavitation dynamics, and laser scattering for the produced materials in the liquid [96]. A diagram of the set-up can be seen in Figure 9 [96]. An Nd:YAG laser (532 nm, 8 ns, 10 Hz) was used for ablation of a solid metal target, in the form of a wire or a solid bulk, in water. By measuring the plasma temperature using OES and the initial volume from the shadowgraph images, the authors could calculate an initial pressure of the cavitation bubble, estimating values of 10^8 Pa for metal bulk targets ablated with laser fluences of 6 J/cm^2. When the bubble reaches its maximum expansion, the temperature of the bubble will be approximately equal to that of the surrounding liquid, and the pressure will be equal to the saturation pressure at that temperature. This pressure will be orders of magnitude lower than the surrounding liquid pressure, causing the bubble to contract. The authors note that this process is important, as produced nanomaterials may be deposited onto the surface of the target instead of being driven out into the solution. The shadowgraph, and laser scattering, images of the process for a titanium target are presented in Figure 0 [96].

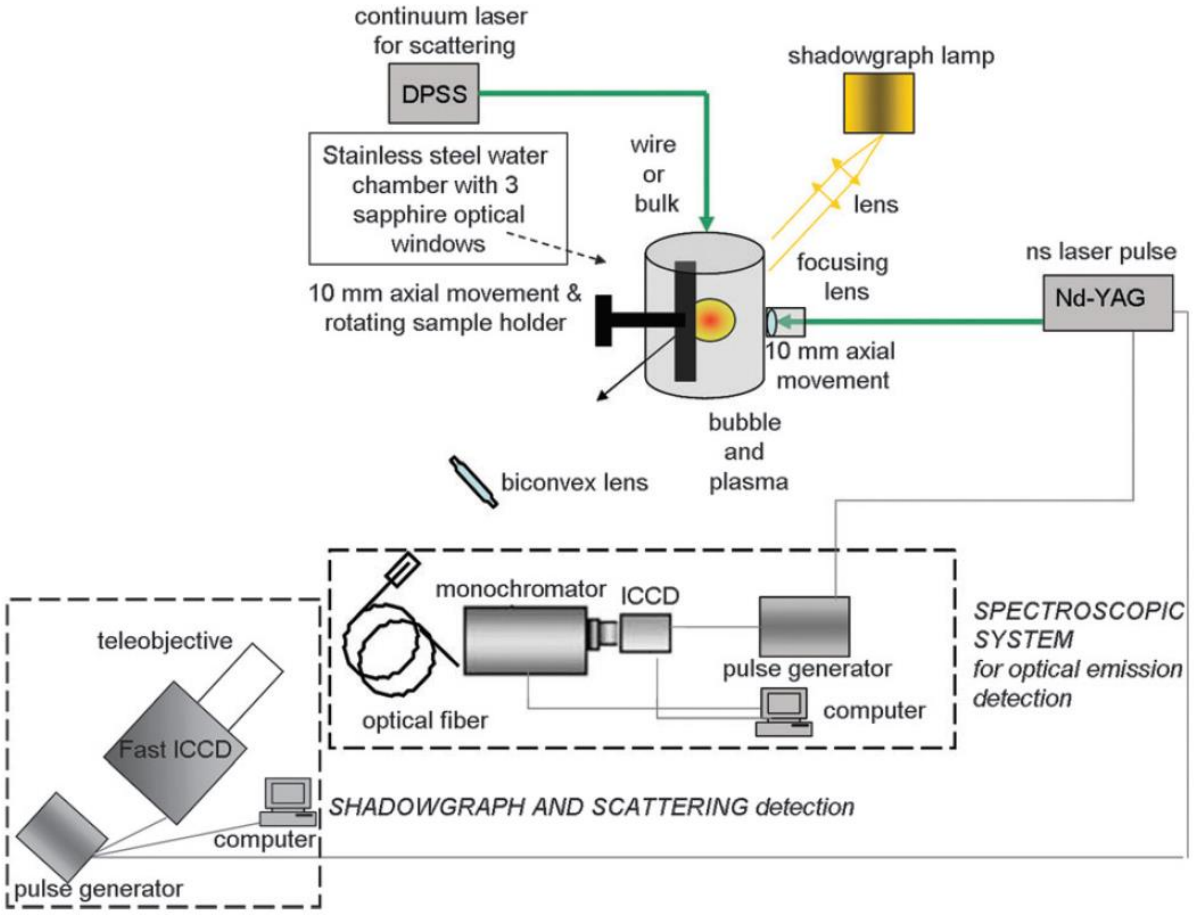

Figure 9: Experimental set-up to monitor PLAL nanoparticle generation using optical emission spectroscopy, shadowgraph, and laser scattering (Reproduced from [96]).

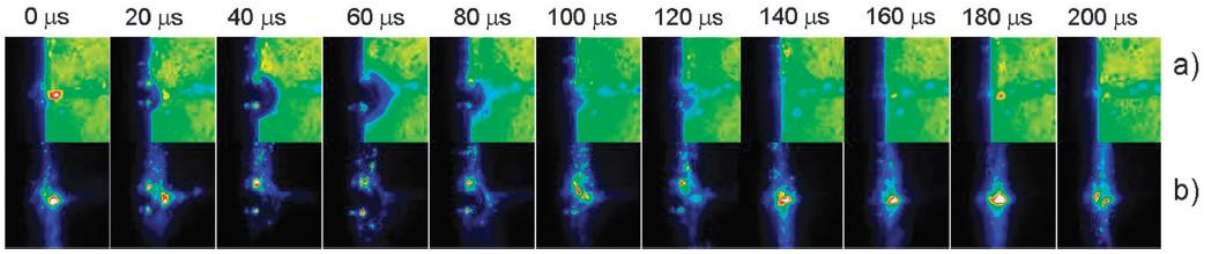

Figure 10: Temporally resolved (a) shadowgraph and (b) laser scattering images of a PLAL bubble on a Ti bulk target in water (Reproduced from [96]).

The bubble reaches maximum expansion around 60 μs, and it can be seen that after collapse there is a rebound bubble. The laser scattering signal indicates the produced particles lie close to the target surface. This is undesirable; as discussed particles may deposit onto the surface of the target. It is more desirable that the produced nanoparticles are ejected into the solution. Post-PLAL scanning electron microscope (SEM) examination of the target showed the

presence of deposited nanoparticles on the surface. Using the bubble radii determined from the shadowgraph images, the authors estimate the pressure and temperature in the cavitation bubble at each observation time using the van der Waals model [96]:

$$P(t) = \left(P_\infty + \frac{2\sigma}{R}\right)\left(\frac{{R_\infty}^3 - h^3}{R^3 - h^3}\right)^\gamma$$

$$T(t) = T_\infty\left(\frac{{R_\infty}^3 - h^3}{R^3 - h^3}\right)^{\gamma-1}$$

where P_∞ and T_∞ are the pressure and temperature of the liquid, R is the bubble radius, R_∞ is the radius at which the pressure in the bubble corresponds to the liquid pressure, σ is the surface tension of the liquid, $h = R_\infty/9.174$, and $\gamma = 1.22$. From this, they estimated that the pressure and temperature in the bubble exceed 1000 K and 10^7 Pa as the bubble collapses. The values they obtain are limited by the time interval of the shadowgraphs compared to the rapid changes of the bubble. Theoretical modelling of laser-induced cavitation bubble collapse by Akhatov et al. has shown internal temperature values of 5000 - 10 000 K, and pressures of thousands of MPa [100]. These high values may be responsible for the deposition of nanoparticles onto the target [96]. Ablation of wire targets was shown to give ejection of the nanoparticles into the solution, unlike the bulk targets, indicating the influence that target shape can have on nanoparticle generation output. For a wire target, the cavitation bubble was found to detach from the surface as it collapses, ejecting the particles. Shadowgraph images for wire targets of increasing thickness and a bulk target can be seen in Figure 21 [96]. The authors suggest this may affect the formation of the colloid, meriting further investigation, but also improves the output/scalability. The process parameters were also related to the results, indicating increased repetition rate improves yield. However, if pulses are delivered before the cavitation bubble created by the previous pulse has collapsed, the target will be shielded from the laser energy by the bubble. The authors estimate, based on the durations determined by shadowgraph, that repetition rates higher than 7 kHz will lead to bubble shielding, and that repetition rates higher than 3 kHz will lead to absorption and scattering by produced nanoparticles, limiting the ablation efficiency.

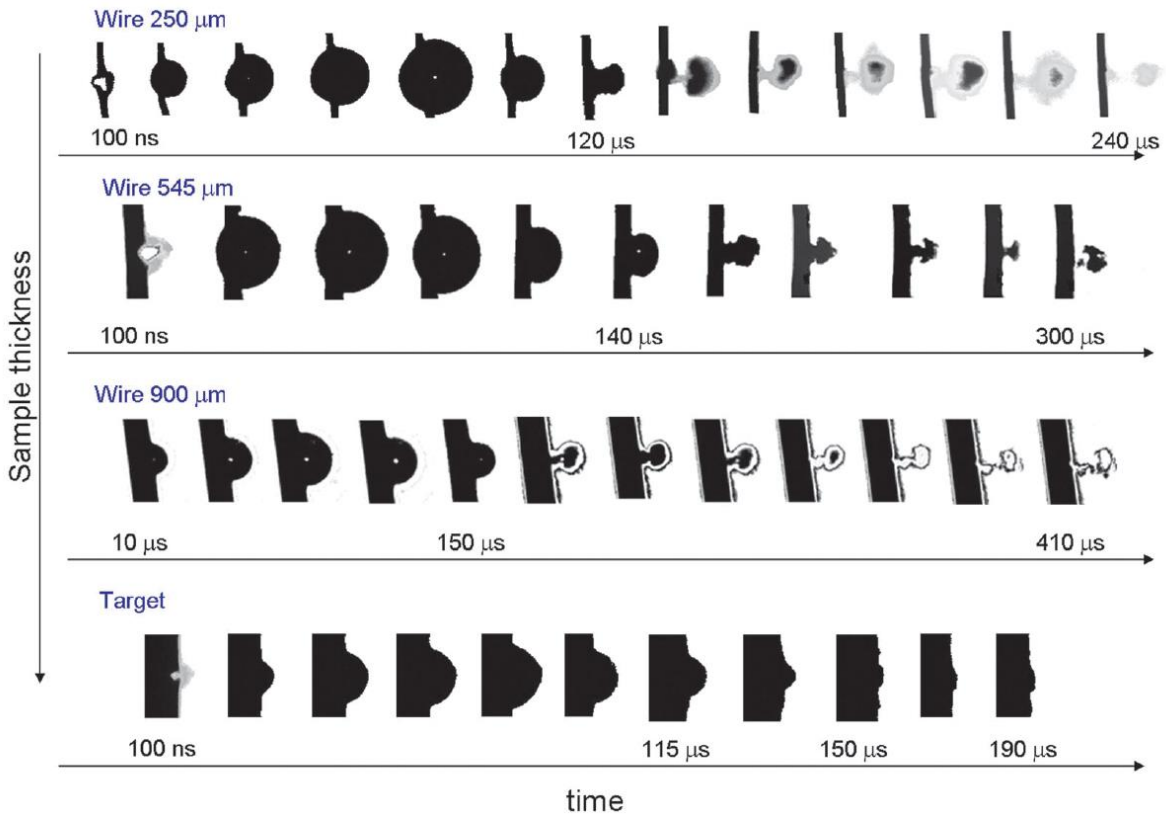

Figure 21: Time-resolved shadowgraph images of PLAL cavitation bubbles for different targets (Reproduced from [96]).

The majority of PLAL is static, or batch, production: ablation of a solid target in a container of liquid. Nanoparticles are produced in a batch, and then the solution must be removed from the container and replaced with fresh solvent. As discussed, the cavitation bubble and ejected nanomaterials may act to shield the ablation target at higher repetition rates [96]. Furthermore, as production continues, the liquid will begin to saturate with nanoparticles, reducing the ablation efficiency. This static approach has the advantage of simplicity, but limits scalability and output. The low productivity for PLAL has been noted as the bottleneck for the method, inhibiting its uptake in industry [111]. This has driven the development of batch and continuous or semi-continuous methods, where the target is immersed in a flow of solvent [112,113].

Barcikowski et al. report on a flow based PLAL method to generate silver nanoparticles [113]. In this method, a magnetic stirrer is utilised to produce flow over the target in a bypass flow cell. While the method is still batch based, the flow of solvent will move nanoparticles, vapour bubbles, and heated liquid away from the ablation site and act to cool the target. A commercial picosecond laser (1064 nm, 10 ps) was focused on a solid

silver target in water in the flow cell, scanning the spot linearly. The experiment was carried out with the same processing parameters for static conditions, for comparison. The authors note that the production rate and nanoparticle size distribution for the static process has poor reproducibility. The authors observed a wavy and inconsistent appearance in the ablation lines on the target used under static conditions, and the effective spot size on the surface was found to be larger due to scattering of the laser light. The production rate was increased by 380% for flow conditions compared with static conditions, with picosecond laser ablation achieving a maximum productivity of 8.6 µg/s.

Messina et al. report the production of silver nanoparticles with a continuously-fed wire target under flow conditions [112]. An Nd:YAG laser (1064 nm, 10 ns) was reduced to a collimated 3 mm using telescope optics and passed through an ablation chamber where a silver wire target (of 125 – 1000 µm diameter) is continuously fed by motor, shown in Figure 12 [112]. The water in the chamber is pumped parallel to the direction of the wire feeding, to avoid bending of the wire by the water pressure, at a flow rate of 9 ml/s. As discussed with Barcikowski et al. [113], the geometry of the target was found to have an effect on ablation efficiency, with wire targets giving higher ablation efficiency than bulk targets due to the release of the cavitation bubble from the surface. There are three main factors related to the diameter of the wire influencing the ablation efficiency: the area irradiated by the laser, and thus the fluence; the heat dispersion, which for cylinders decreases with decreasing diameter and will also be affected by the thermal diffusivity of the material; and that for large enough diameters the cavitation bubble behaviour will approach that of a bulk target, with the bubble remaining on the surface as it collapses. In all cases, the wire targets had higher ablation efficiency than a bulk target, and the 750 µm diameter wire was found to give the best efficiency, increased by a factor of 15 compared to a bulk target. Productivity also increased linearly with repetition rates tested, from 1-100 Hz, as the interval between pulses was longer than the lifetime of the cavitation bubble (~250 µs). The linear increase should continue, until the interval impinges on the duration of bubble, with maximum repetition rates of about 2 kHz. The authors estimate for higher repetition rates a theoretical maximal productivity of >25 g/h should be achievable with a 750 µm diameter wire target. Fluence (0.4-1.5 J/cm^2) was also found to have a linear relationship with the productivity. The silver nanoparticles produced had sizes ranging 15-20 nm, with no difference between those produced from wire and bulk targets, indicating that the temperature and pressure in the cavitation bubble were not affected by the geometry [96,112].

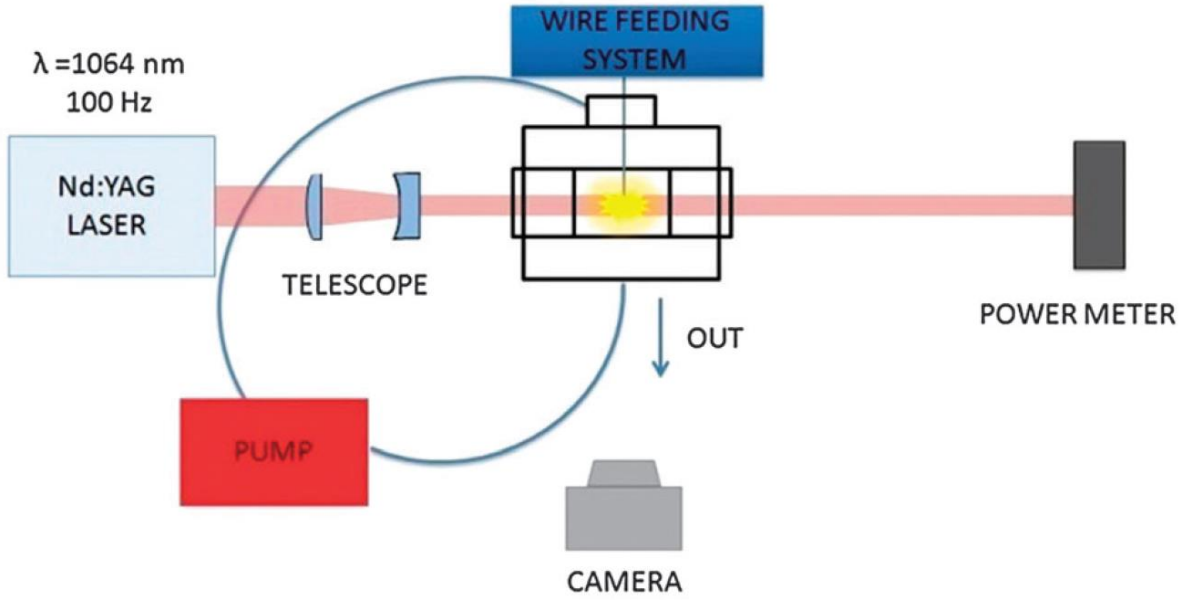

Figure 12: Experimental setup for continuous wire target PLAL (Reproduced from [112]).

Streubel et al. describe a high speed PLAL process for continuous metal nanoparticle generation [111]. A picosecond laser (1030 nm, 3 ps, 10 MHz, 500 W) combined with a polygon scanner was used to scan the laser spot at speeds of up to 500 m/s over metal (platinum, silver, gold, aluminium, copper, and titanium) targets under flow conditions. With high scanning speeds, a subsequent pulse can be spatially removed from its prior pulse, allowing higher repetition rates to be used without the issue of cavitation bubble shielding. The authors acknowledge the productivity bottleneck facing PLAL, and point out that studies which report ablation rates ≥ 1 g/h often extrapolate from rates measured over seconds or minutes [114,115]. Schwenke et al. investigated the influence of processing time on nanoparticle generation [116]. In this work they studied ablation rates by picosecond PLAL for times of up to 1 hour. They found evidence that ablated mass did not increase linearly with ablation time, attributed to the absorption or scattering of laser light by the produced nanoparticles, indicating that extrapolating from seconds or minutes of ablation may not be valid. In the work by Streubel et al., bypassing of cavitation bubble and nanoparticle shielding using an advanced beam scanner and flow conditions presents an opportunity to achieve high productivity over long time frames (see Figure 13) [111]. An ultrafast laser beam is directed by two scanning systems, a polygon scanner for fast, vertical translation, and a galvanometric mirror for slower, horizontal translation. Water is pumped through the

ablation chamber, with the colloid being collected in a different vessel, allowing for semi-continuous production. The authors carried out optimisation experiments with 10 minute durations to optimise the process parameters, then used the optimised parameters (500 W, 10.1 MHz, 484 m/s) for 1 hour of continuous production for six different metal targets (platinum, gold, silver, aluminium, copper, and titanium). The resulting production rates are presented in Figure 14 [111]. The highest productivity achieved was 4.1 g/h, for the platinum target.

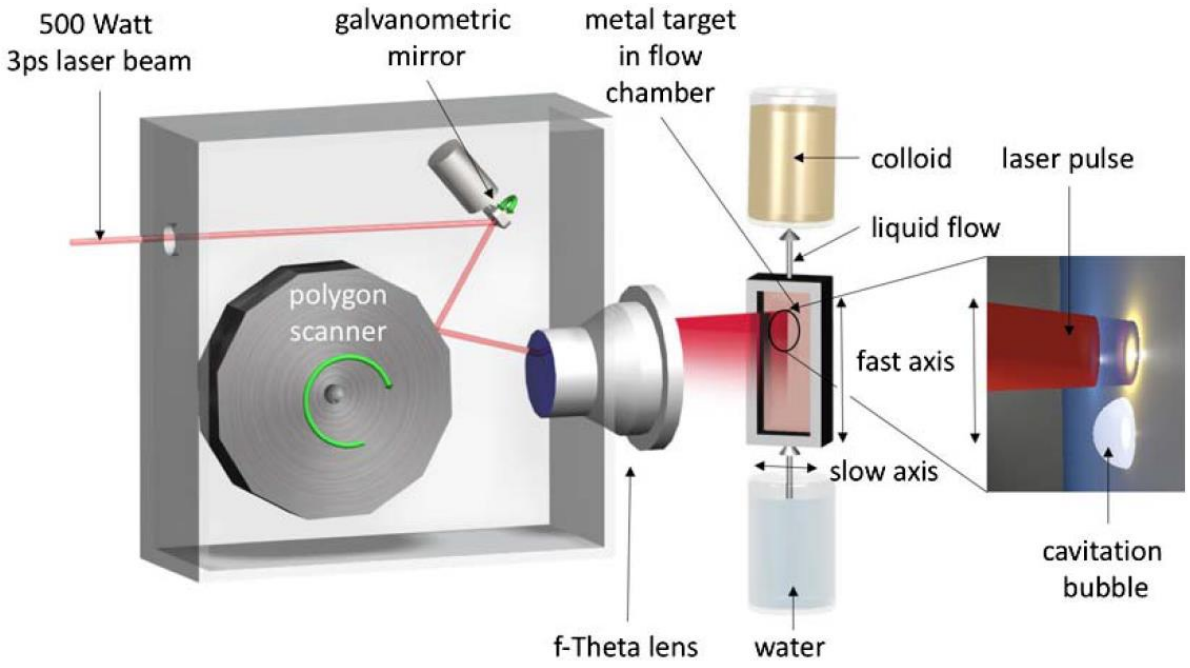

Figure 13: Ultrafast polygon scanner PLAL process for continuous metal nanoparticle generation, with a magnified insert showing the spatial bypassing of cavitation bubble shielding (Reproduced from [111]).

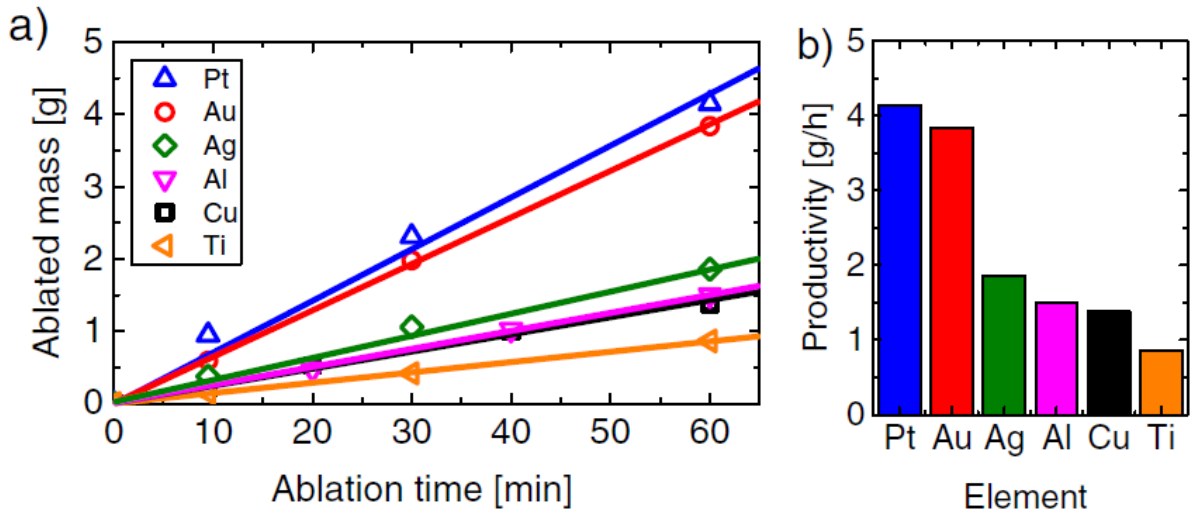

Figure 14: Productivities for fast scan PLAL (a) ablated mass as a function of time for six metal targets (b) the productivity in g/h for the different targets (Reproduced from [111]).

Another factor affecting the yield for PLAL is the thickness of the liquid layer covering the target [117–119]. As light travels through a liquid medium some of the light will be absorbed, attenuating the beam, with thicker layers of water leading to a greater portion of the laser energy being absorbed. However, if the liquid layer is too thin it may insufficiently confine the plasma plume, even allowing the plume to expand beyond the surface of the liquid [119]. Jiang et al. investigated the yield for PLAL generation of germanium nanoparticles in deionised water using a 532 nm wavelength Nd:YAG laser [118]. They found the optimum water layer thickness for these conditions to be 1.2 mm.

Kohsakowski et al. report on a continuous method for nanoparticle generation using wire-targets in a liquid jet [102]. Previous works have shown the increased effectiveness and productivity of wire targets [112,113]. Kohsakowski et al. present an experimental method for PLAL nanoparticle generation in which a wire target is continuously fed, as in Messina et al. [112], under a liquid jet. This method combines continuous liquid flow, with a thin liquid layer, a wire target geometry, and continuous feeding of the target. The experimental setup is shown in Figure 15[102]. Wires of different materials and diameters could be fed through the jet nozzle, with interchangeable nozzles of 1-4 mm diameter to allow varying of the liquid layer thickness. Water flow was controlled by pump to give a flow rate of up to 8 mL/s, and the layer thickness was measured by imaging with a camera system. A nanosecond Nd:YAG laser (1064 nm, 0.1 - 15 kHz, 2-8 mJ per pulse) was used for the ablation. A power meter

behind the jet was used to ensure good illumination of the wire target by minimising the power detected.

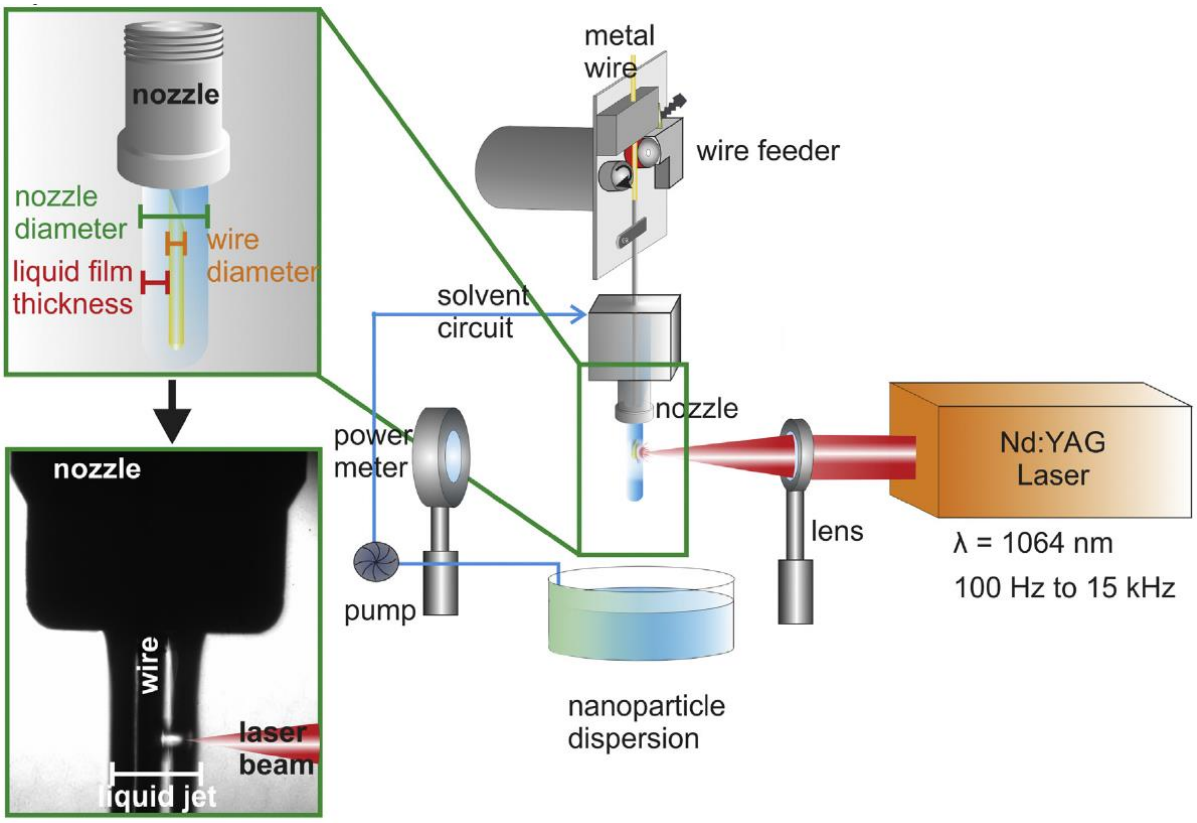

Figure 15: Experimental setup for continuous PLAL using a continuously fed wire target and water jet (Reproduced from [102]).

The authors determined the process was successful as a continuous and stable nanoparticle production process, with consistent particle sizes. High productivities were obtained, over a 1 hour process time: 220, 410, and 550 mg/h for gold, platinum, and silver, respectively. The values are lower than those obtained by Streubel et al. [111], however Kohsakowski et al. were applying a nanosecond pulse with 32.5 W laser power, compared to Streubel et al. using picosecond pulses with 250 W laser power. The power specific productivity, in terms of the ablated mass per unit of laser power, was comparable for the two works; ranging 6.77 to 16.92 mg/hW for Kohsakowski et al., and 7.6 to 16.20 mg/hW for Streubel et al. [102,111]. Highest productivities were found with a liquid layer thickness of 500 µm.

5 Conclusions

In this chapter, we presented a review of the applications of nanoparticles, a general overview of the generation methods, and a specific review of the PLAL method. PLAL is a useful approach for producing nanomaterials in solution. Control of the processing parameters allows the production of a wide range of sizes and morphologies (nanoparticles, nanorods, etc.), and is applicable to a wide range of target materials. The method typically avoids the use of hazardous, environmentally unfriendly chemicals, and produces ligand-free nanoparticles which are necessary for many applications.

The main limitation for PLAL has been achieving high, commercially-viable, production rates. A number of cutting edge PLAL approaches reviewed here, such as stirred batch, dynamic flow based, high-speed polygon scanning, and wire in liquid jet production have led to success with providing greatly improved production rates, which provide the much-needed scalability, enabling the implementation of PLAL as a more commercially-viable nanoparticle production method.

Acknowledgements

This research is supported by a research grant from Science Foundation Ireland (SFI) under Grant Number 16/RC/3872 and 19/US-C2C/3579; and is co-funded under the European Regional Development Fund.

Bibliography

[1] Navrotsky A. Thermochemistry of nanomaterials. Rev Mineral Geochemistry 2001;44:73–103. doi:10.2138/rmg.2001.44.03.

[2] Balasubramanian K. Challenges in the use of 1D nanostructures for on-chip biosensing and diagnostics: A review. Biosens Bioelectron 2010;26:1195–204. doi:10.1016/j.bios.2010.07.041.

[3] Tonezzer M, Dang TT Le, Bazzanella N, Nguyen VH, Iannotta S. Comparative gas-sensing performance of 1D and 2D ZnO nanostructures. Sensors Actuators, B Chem 2015;220:1152–60. doi:10.1016/j.snb.2015.06.103.

[4] Liu FK. Analysis and applications of nanoparticles in the separation sciences: A case of gold nanoparticles. J Chromatogr A 2009;1216:9034–47. doi:10.1016/j.chroma.2009.07.026.

[5] Park JB, Lee KH, Jeon YJ, Lim SH, Lee SM. Si/C composite lithium-ion battery anodes synthesized using silicon nanoparticles from porous silicon. Electrochim Acta 2014;133:73–81.

doi:10.1016/j.electacta.2014.04.045.

[6] Yu YH, Ma CCM, Teng CC, Huang YL, Lee SH, Wang I, et al. Electrical, morphological, and electromagnetic interference shielding properties of silver nanowires and nanoparticles conductive composites. Mater Chem Phys 2012;136:334–40. doi:10.1016/j.matchemphys.2012.05.024.

[7] Bagga K, McCann R, Wang M, Stalcup a, Vázquez M, Brabazon D. Laser assisted synthesis of carbon nanoparticles with controlled viscosities for printing applications. J Colloid Interface Sci 2014. doi:10.1016/j.jcis.2014.10.046.

[8] Haidary SM, Córcoles EP, Ali NK. Nanoporous silicon as drug delivery systems for cancer therapies. J Nanomater 2012;2012. doi:10.1155/2012/830503.

[9] Weber J, Singhal R, Zekri S, Kumar A. One-dimensional nanostructures: fabrication, characterisation and applications. Int Mater Rev 2008;53:235–55. doi:10.1179/174328008X348183.

[10] Ahmad M, Kiely J, Luxton R, Jabeen M, Khalid M. Facile aqueous growth of 150 nm ZnO nanowires for energy harvester: Enhanced output voltage using Pt sputtered electrode. Sens Bio-Sensing Res 2016;7:141–5. doi:10.1016/j.sbsr.2015.12.005.

[11] Ahmad M, Iqbal MA, Kiely J, Luxton R, Jabeen M. Enhanced output voltage generation via ZnO nanowires (50 nm): Effect of diameter thinning on voltage enhancement. J Phys Chem Solids 2017;104:281–5. doi:10.1016/j.jpcs.2017.01.006.

[12] Sahay S, Kumar MJ. Diameter Dependence of Leakage Current in Nanowire Junctionless Field Effect Transistors. IEEE Trans Electron Devices 2017;64:1330. doi:10.1109/TED.2016.2645640.

[13] Dreaden EC, Alkilany AM, Huang X, Murphy CJ, El-Sayed MA. The golden age: Gold nanoparticles for biomedicine. Chem Soc Rev 2012;41:2740–79. doi:10.1039/c1cs15237h.

[14] Barcikowski S, Compagnini G. Advanced nanoparticle generation and excitation by lasers in liquids. Phys Chem Chem Phys 2013;15:3022–6. doi:10.1039/c2cp90132c.

[15] Li Y, Wang Z, Sun L, Liu L, Xu C, Kuang H. Nanoparticle-based sensors for food contaminants. TrAC - Trends Anal Chem 2019;113:74–83. doi:10.1016/j.trac.2019.01.012.

[16] El-Ansary A, Faddah LM. Nanoparticles as biochemical sensors. Nanotechnol Sci Appl 2010;3:65–76. doi:10.2147/NSA.S8199.

[17] Sharma R, Ragavan K V., Thakur MS, Raghavarao KSMS. Recent advances in nanoparticle based aptasensors for food contaminants. Biosens Bioelectron 2015;74:612–27. doi:10.1016/j.bios.2015.07.017.

[18] Deng J, Yu P, Wang Y, Yang L, Mao L. Visualization and quantification of neurochemicals with gold nanoparticles: Opportunities and challenges. Adv Mater 2014;26:6933–43. doi:10.1002/adma.201305619.

[19] Bigdeli A, Ghasemi F, Golmohammadi H, Abbasi-Moayed S, Nejad MAF, Fahimi-Kashani N, et al. Nanoparticle-based optical sensor arrays. Nanoscale 2017;9:16546–63. doi:10.1039/c7nr03311g.

[20] Liu D, Wang Z, Jiang X. Gold nanoparticles for the colorimetric and fluorescent detection of ions and small organic molecules. Nanoscale 2011;3:1421–33. doi:10.1039/c0nr00887g.

[21] Chen XY, Ha W, Shi YP. Sensitive colorimetric detection of melamine in processed raw milk using asymmetrically PEGylated gold nanoparticles. Talanta 2019;194:475–84. doi:10.1016/j.talanta.2018.10.070.

[22] Lam CW, Lan L, Che X, Tam S, Wong SSY, Chen Y, et al. Diagnosis and spectrum of melamine-related renal disease: Plausible mechanism of stone formation in humans. Clin Chim Acta 2009;402:150–5. doi:10.1016/j.cca.2008.12.035.

[23] Ramezani M, Mohammad Danesh N, Lavaee P, Abnous K, Mohammad Taghdisi S. A novel colorimetric triple-helix molecular switch aptasensor for ultrasensitive detection of tetracycline. Biosens Bioelectron 2015;70:181–7. doi:10.1016/j.bios.2015.03.040.

[24] Ruedas-Rama MJ, Walters JD, Orte A, Hall EAH. Fluorescent nanoparticles for intracellular sensing: A review. Anal Chim Acta 2012;751:1–23. doi:10.1016/j.aca.2012.09.025.

[25] Xu J, Li Y, Wang L, Huang Y, Liu D, Sun R, et al. A facile aptamer-based sensing strategy for dopamine through the fluorescence resonance energy transfer between rhodamine B and gold nanoparticles. Dye Pigment 2015;123:55–63. doi:10.1016/j.dyepig.2015.07.019.

[26] Konduru T, Rains GC, Li C. A customized metal oxide semiconductor-based gas sensor array for onion quality evaluation: system development and characterization. Sensors (Basel) 2015;15:1252–73. doi:10.3390/s150101252.

[27] Cigić IK, Prosen H. An overview of conventional and emerging analytical methods for the determination of mycotoxins. Int J Mol Sci 2009;10:62–115. doi:10.3390/ijms10010062.

[28] Vargas-Bernal R, Rodrguez-Miranda E, Herrera-Prez G. Evolution and Expectations of Enzymatic Biosensors for Pesticides. Pestic - Adv Chem Bot Pestic 2012. doi:10.5772/46227.

[29] Yusoff N, Pandikumar A, Ramaraj R, Lim HN, Huang NM. Gold nanoparticle based optical and electrochemical sensing of dopamine. Microchim Acta 2015;182:2091–114. doi:10.1007/s00604-015-1609-2.

[30] Raj CR, Okajima T, Ohsaka T. Gold nanoparticle arrays for the voltammetric sensing of dopamine. J Electroanal Chem 2003;543:127–33. doi:10.1016/S0022-0728(02)01481-X.

[31] Cruz SMF, Rocha LA, Viana JC. Printing Technologies on Flexible Substrates for Printed Electronics. Flex. Electron., IntechOpen; 2018. doi:http://dx.doi.org/10.5772/57353.

[32] Nayak L, Mohanty S, Nayak SK, Ramadoss A. A review on inkjet printing of nanoparticle inks for flexible electronics. J Mater Chem C 2019;7:8771–95. doi:10.1039/c9tc01630a.

[33] Gao Y, Liu R, Wang X, Liu J, Fang Q. Flexible RFID Tag Inductor Printed by Liquid Metal Ink Printer and Its Characterization. J Electron Packag 2016;138:031007. doi:10.1115/1.4034062.

[34] Kopyt P, Salski B, Olszewska M, Janczak D, Sloma M, Kurkus T, et al. Graphene-based dipole antenna for a UHF RFID tag. 2015 IEEE MTT-S Int Microw Symp 2015;1:1–3. doi:10.1109/MWSYM.2015.7166755.

[35] Leng T, Huang X, Chang K, Chen J, Abdalla MA, Hu Z. Graphene Nanoflakes Printed Flexible Meandered-Line Dipole Antenna on Paper Substrate for Low-Cost RFID and Sensing Applications. IEEE Antennas Wirel Propag Lett 2016;15:1565–8. doi:10.1109/LAWP.2016.2518746.

[36] Matyas J, Munster L, Olejnik R, Vlcek K, Slobodian P, Krcmar P, et al. Antenna of silver nanoparticles mounted on a flexible polymer substrate constructed using inkjet print technology. Jpn J Appl Phys 2016;55:02BB13. doi:10.7567/JJAP.55.02BB13.

[37] Jeong S, Song HC, Lee WW, Lee SS, Choi Y, Son W, et al. Stable aqueous based Cu nanoparticle ink for printing well-defined highly conductive features on a plastic substrate. Langmuir 2011;27:3144–9.

doi:10.1021/la104136w.

[38] Duval JF, Herr HM. FlexSEA: Flexible, Scalable Electronics Architecture for wearable robotic applications. Proc IEEE RAS EMBS Int Conf Biomed Robot Biomechatronics 2016;2016-July:1236–41. doi:10.1109/BIOROB.2016.7523800.

[39] Cheng MY, Lin CL, Yang YJ. Tactile and shear stress sensing array using capacitive mechanisms with floating electrodes. Proc IEEE Int Conf Micro Electro Mech Syst 2010;2:228–31. doi:10.1109/MEMSYS.2010.5442525.

[40] Chiang CC, K. Lin CC, Ju MS. An implantable capacitive pressure sensor for biomedical applications. Sensors Actuators, A Phys 2007;134:382–8. doi:10.1016/j.sna.2006.06.007.

[41] Kim K, Kim B, Lee CH. Printing Flexible and Hybrid Electronics for Human Skin and Eye-Interfaced Health Monitoring Systems. Adv Mater 2019;1902051:1–22. doi:10.1002/adma.201902051.

[42] Komoda N, Nogi M, Suganuma K, Kohno K, Akiyama Y, Otsuka K. Printed silver nanowire antennas with low signal loss at high-frequency radio. Nanoscale 2012;4:3148. doi:10.1039/c2nr30485f.

[43] He H, Sydänheimo L, Virkki J, Ukkonen L. Experimental Study on Inkjet-Printed Passive UHF RFID Tags on Versatile Paper-Based Substrates 2016;2016:1–9.

[44] Sydanheimo L, Virkki J, Ukkonen L, Ren Y. Optimisation of manufacturing parameters for inkjet-printed and photonically sintered metallic nanoparticle UHF RFID tags. Electron Lett 2014;50:1504–5. doi:10.1049/el.2014.2194.

[45] Chen B, Jiang Y, Tang X, Pan Y, Hu S. Fully Packaged Carbon Nanotube Supercapacitors by Direct Ink Writing on Flexible Substrates. ACS Appl Mater Interfaces 2017;9:28433–40. doi:10.1021/acsami.7b06804.

[46] Rajan K, Roppolo I, Chiappone A, Bocchini S, Perrone D, Chiolerio A. Nanotechnology, Science and Applications Dovepress Silver nanoparticle ink technology: state of the art. Nanotechnol Sci Appl 2016;9:1–13. doi:10.2147/NSA.S68080.

[47] Balliu E, Andersson H, Engholm M, Öhlund T, Nilsson HE, Olin H. Selective laser sintering of inkjet-printed silver nanoparticle inks on paper substrates to achieve highly conductive patterns. Sci Rep 2018;8:2–10. doi:10.1038/s41598-018-28684-4.

[48] Taufik S, Barfidokht A, Alam MT, Jiang C, Parker SG, Gooding JJ. An antifouling electrode based on electrode–organic layer–nanoparticle constructs: Electrodeposited organic layers versus self-assembled monolayers. J Electroanal Chem 2016;779:229–35. doi:10.1016/j.jelechem.2016.01.031.

[49] Nguyen A, Zou L, Priest C. Evaluating the antifouling effects of silver nanoparticles regenerated by TiO2 on forward osmosis membrane. J Memb Sci 2014;454:264–71. doi:10.1016/j.memsci.2013.12.024.

[50] Kirschner CM, Brennan AB. Bio-Inspired Antifouling Strategies. Annu Rev Mater Res 2012;42:211–29. doi:10.1146/annurev-matsci-070511-155012.

[51] Yu B, Leung KM, Guo Q, Lau WM, Yang J. Synthesis of Ag-TiO2 composite nano thin film for antimicrobial application. Nanotechnology 2011;22. doi:10.1088/0957-4484/22/11/115603.

[52] Schacht VJ, Neumann L V., Sandhi SK, Chen L, Henning T, Klar PJ, et al. Effects of silver nanoparticles on microbial growth dynamics. J Appl Microbiol 2013;114:25–35. doi:10.1111/jam.12000.

[53] Yang HL, Lin JC Te, Huang C. Application of nanosilver surface modification to RO membrane and spacer for mitigating biofouling in seawater desalination. Water Res 2009;43:3777–86. doi:10.1016/j.watres.2009.06.002.

[54] Sondi I, Salopek-Sondi B. Silver nanoparticles as antimicrobial agent: A case study on E. coli as a model for Gram-negative bacteria. J Colloid Interface Sci 2004;275:177–82. doi:10.1016/j.jcis.2004.02.012.

[55] Marambio-Jones C, Hoek EMV. A review of the antibacterial effects of silver nanomaterials and potential implications for human health and the environment. J Nanoparticle Res 2010;12:1531–51. doi:10.1007/s11051-010-9900-y.

[56] AshaRani PV, Mun GLK, Hande MP, Valiyaveettil S. Cytotoxicity and genotoxicity of silver nanomaterials. ACS Nano 2009;3:279–90. doi:10.1021/nn800596w.

[57] Lok CN, Ho CM, Chen R, He QY, Yu WY, Sun H, et al. Silver nanoparticles: Partial oxidation and antibacterial activities. J Biol Inorg Chem 2007;12:527–34. doi:10.1007/s00775-007-0208-z.

[58] Pi JK, Yang HC, Wan LS, Wu J, Xu ZK. Polypropylene microfiltration membranes modified with TiO2 nanoparticles for surface wettability and antifouling property. J Memb Sci 2016;500:8–15. doi:10.1016/j.memsci.2015.11.014.

[59] de la Torre C, Ceña V. The delivery challenge in neurodegenerative disorders: The nanoparticles role in alzheimer's disease therapeutics and diagnostics. Pharmaceutics 2018;10. doi:10.3390/pharmaceutics10040190.

[60] Wen MM, El-Salamouni NS, El-Refaie WM, Hazzah HA, Ali MM, Tosi G, et al. Nanotechnology-based drug delivery systems for Alzheimer's disease management: Technical, industrial, and clinical challenges. J Control Release 2017;245:95–107. doi:10.1016/j.jconrel.2016.11.025.

[61] Cunha S, Amaral M, Lobo J, Silva A. Therapeutic Strategies for Alzheimer's and Parkinson's Diseases by Means of Drug Delivery Systems. Curr Med Chem 2016;23:3618–31. doi:10.2174/0929867323666160824162401.

[62] Xiao Y, Shi K, Qu Y, Chu B, Qian Z. Engineering Nanoparticles for Targeted Delivery of Nucleic Acid Therapeutics in Tumor. Mol Ther - Methods Clin Dev 2019;12:1–18. doi:10.1016/j.omtm.2018.09.002.

[63] Singh P, Pandit S, Mokkapati VRSS, Garg A, Ravikumar V, Mijakovic I. Gold nanoparticles in diagnostics and therapeutics for human cancer. Int J Mol Sci 2018;19. doi:10.3390/ijms19071979.

[64] Hui Y, Yi X, Hou F, Wibowo D, Zhang F, Zhao D, et al. Role of Nanoparticle Mechanical Properties in Cancer Drug Delivery. ACS Nano 2019;13:7410–24. doi:10.1021/acsnano.9b03924.

[65] Lewis DR, Kamisoglu K, York AW, Moghe P V. Polymer-based therapeutics: Nanoassemblies and nanoparticles for management of atherosclerosis. Wiley Interdiscip Rev Nanomedicine Nanobiotechnology 2011;3:400–20. doi:10.1002/wnan.145.

[66] Bharali DJ, Klejbor I, Stachowiak EK, Dutta P, Roy I, Kaur N, et al. Organically modified silica nanoparticles: A nonviral vector for in vivo gene delivery and expression in the brain. Proc Natl Acad Sci U S A 2005;102:11539–44. doi:10.1073/pnas.0504926102.

[67] Huang X, El-Sayed MA. Plasmonic photo-thermal therapy (PPTT). Alexandria J Med 2011;47:1–9. doi:10.1016/j.ajme.2011.01.001.

[68] Ali MRK, Wu Y, El-Sayed MA. Gold-Nanoparticle-Assisted Plasmonic Photothermal Therapy

Advances Toward Clinical Application. J Phys Chem C 2019;123:15375–93. doi:10.1021/acs.jpcc.9b01961.

[69] Napier ME, DeSimone JM. Nanoparticle drug delivery platform. Polym Rev 2007;47:321–7. doi:10.1080/15583720701454999.

[70] Liu M, Song W, Huang L. Drug delivery systems targeting tumor-associated fibroblasts for cancer immunotherapy. Cancer Lett 2019;448:31–9. doi:10.1016/j.canlet.2019.01.032.

[71] Bahrami B, Hojjat-Farsangi M, Mohammadi H, Anvari E, Ghalamfarsa G, Yousefi M, et al. Nanoparticles and targeted drug delivery in cancer therapy. Immunol Lett 2017;190:64–83. doi:10.1016/j.imlet.2017.07.015.

[72] Kong FY, Zhang JW, Li RF, Wang ZX, Wang WJ, Wang W. Unique roles of gold nanoparticles in drug delivery, targeting and imaging applications. Molecules 2017;22. doi:10.3390/molecules22091445.

[73] Ajnai G, Chiu A, Kan T, Cheng CC, Tsai TH, Chang J. Trends of Gold Nanoparticle-based Drug Delivery System in Cancer Therapy. J Exp Clin Med 2014;6:172–8. doi:10.1016/j.jecm.2014.10.015.

[74] Chen YH, Tsai CY, Huang PY, Chang MY, Cheng PC, Chou CH, et al. Methotrexate conjugated to gold nanoparticles inhibits tumor growth in a syngeneic lung tumor model. Mol Pharm 2007;4:713–22. doi:10.1021/mp060132k.

[75] Wechsler ME, Vela Ramirez JE, Peppas NA. 110th Anniversary : Nanoparticle Mediated Drug Delivery for the Treatment of Alzheimer's Disease: Crossing the Blood–Brain Barrier . Ind Eng Chem Res 2019;58:15079–87. doi:10.1021/acs.iecr.9b02196.

[76] Han P, Martens W, Waclawik ER, Sarina S, Zhu H. Metal Nanoparticle Photocatalysts: Synthesis, Characterization, and Application. Part Part Syst Charact 2018;35:1–16. doi:10.1002/ppsc.201700489.

[77] Wiley B, Sun Y, Mayers B, Xia Y. Shape-controlled synthesis of metal nanostructures: The case of silver. Chem - A Eur J 2005;11:454–63. doi:10.1002/chem.200400927.

[78] Iravani S, Korbekandi H, Mirmohammadi S V., Zolfaghari B. Synthesis of silver nanoparticles: Chemical, physical and biological methods. Res Pharm Sci 2014;9:385–406.

[79] Oliveira MM, Ugarte D, Zanchet D, Zarbin AJG. Influence of synthetic parameters on the size, structure, and stability of dodecanethiol-stabilized silver nanoparticles. J Colloid Interface Sci 2005;292:429–35. doi:10.1016/j.jcis.2005.05.068.

[80] Zhao P, Li N, Astruc D. State of the art in gold nanoparticle synthesis. Coord Chem Rev 2013;257:638–65. doi:10.1016/j.ccr.2012.09.002.

[81] Turkevich J, Stevenson PC, Hillier J. A study of the nucleation and growth processes in the synthesis of colloidal gold. Discuss Faraday Soc 1951;11:55–75. doi:10.1039/DF9511100055.

[82] Frens G. Controlled Nucleation for the Regulation of the Particle Size in Monodisperse Gold Suspensions. Nat Phys Sci 1973;241:20–2. doi:10.1038.

[83] Brown KR, Fox AP, Natan MJ. Morphology-dependent electrochemistry of cytochrome c at Au colloid-modified SnO2 electrodes. J Am Chem Soc 1996;118:1154–7. doi:10.1021/ja952951w.

[84] Roy A, Bulut O, Some S, Mandal AK, Yilmaz MD. Green synthesis of silver nanoparticles: Biomolecule-nanoparticle organizations targeting antimicrobial activity. RSC Adv 2019;9:2673–702. doi:10.1039/c8ra08982e.

[85] Mittal AK, Chisti Y, Banerjee UC. Synthesis of metallic nanoparticles using plant extracts. Biotechnol

Adv 2013;31:346–56. doi:10.1016/j.biotechadv.2013.01.003.

[86] Li X, Xu H, Chen ZS, Chen G. Biosynthesis of nanoparticles by microorganisms and their applications. J Nanomater 2011;2011. doi:10.1155/2011/270974.

[87] Dwivedi AD, Gopal K. Biosynthesis of silver and gold nanoparticles using Chenopodium album leaf extract. Colloids Surfaces A Physicochem Eng Asp 2010;369:27–33. doi:10.1016/j.colsurfa.2010.07.020.

[88] Magnusson MH, Deppert K, Malm JO, Bovin JO, Samuelson L. Gold nanoparticles: Production, reshaping, and thermal charging. J Nanoparticle Res 1999;1:243–51. doi:10.1023/A:1010012802415.

[89] Lo CH, Tsung TT, Lin HM. Preparation of silver nanofluid by the submerged arc nanoparticle synthesis system (SANSS). J Alloys Compd 2007;434–435:659–62. doi:10.1016/j.jallcom.2006.08.217.

[90] Lung JK, Huang JC, Tien DC, Liao CY, Tseng KH, Tsung TT, et al. Preparation of gold nanoparticles by arc discharge in water. J Alloys Compd 2007;434–435:655–8. doi:10.1016/j.jallcom.2006.08.213.

[91] Wang LL, Jiang J Sen. Preparation of α-Fe2O3 nanoparticles by high-energy ball milling. Phys B Condens Matter 2007;390:23–7. doi:10.1016/j.physb.2006.07.043.

[92] Pimpang P, Sutham W, Mangkorntong N, Mangkorntong P, Choopun S. Effect of stabilizer on preparation of silver and gold nanoparticle using grinding method. Chiang Mai J Sci 2008;35:250–7.

[93] Arbain R, Othman M, Palaniandy S. Preparation of iron oxide nanoparticles by mechanical milling. Miner Eng 2011;24:1–9. doi:10.1016/j.mineng.2010.08.025.

[94] Knieke C, Steinborn C, Romeis S, Peukert W, Breitung-Faes S, Kwade A. Nanoparticle production with stirred-media mills: Opportunities and limits. Chem Eng Technol 2010;33:1401–11. doi:10.1002/ceat.201000105.

[95] Baláž M, Balážová Ľ, Daneu N, Dutková E, Balážová M, Bujňáková Z, et al. Plant-Mediated Synthesis of Silver Nanoparticles and Their Stabilization by Wet Stirred Media Milling. Nanoscale Res Lett 2017;12. doi:10.1186/s11671-017-1860-z.

[96] De Giacomo A, Dell'Aglio M, Santagata A, Gaudiuso R, De Pascale O, Wagener P, et al. Cavitation dynamics of laser ablation of bulk and wire-shaped metals in water during nanoparticles production. Phys Chem Chem Phys 2013;15:3083–92. doi:10.1039/c2cp42649h.

[97] Dell'Aglio M, Gaudiuso R, De Pascale O, De Giacomo A. Mechanisms and processes of pulsed laser ablation in liquids during nanoparticle production. Appl Surf Sci 2015;348:4–9. doi:10.1016/j.apsusc.2015.01.082.

[98] Lauterborn W, Kurz T. Physics of bubble oscillations. Reports Prog Phys 2010;73. doi:10.1088/0034-4885/73/10/106501.

[99] Petkovšek R, Gregorčič P. A laser probe measurement of cavitation bubble dynamics improved by shock wave detection and compared to shadow photography. J Appl Phys 2007;102. doi:10.1063/1.2774000.

[100] Akhatov I, Lindau O, Topolnikov A, Mettin R, Vakhitova N, Lauterborn W. Collapse and rebound of a laser-induced cavitation bubble. Phys Fluids 2001;13:2805–19. doi:10.1063/1.1401810.

[101] Zeng H, Du XW, Singh SC, Kulinich SA, Yang S, He J, et al. Nanomaterials via laser ablation/irradiation in liquid: A review. Adv Funct Mater 2012;22:1333–53. doi:10.1002/adfm.201102295.

[102] Kohsakowski S, Santagata A, Dell'Aglio M, de Giacomo A, Barcikowski S, Wagener P, et al. High productive and continuous nanoparticle fabrication by laser ablation of a wire-target in a liquid jet. Appl Surf Sci 2017;403:487–99. doi:10.1016/j.apsusc.2017.01.077.

[103] Ibrahimkutty S, Wagener P, Menzel A, Plech A, Barcikowski S. Nanoparticle formation in a cavitation bubble after pulsed laser ablation in liquid studied with high time resolution small angle x-ray scattering. Appl Phys Lett 2012;101. doi:10.1063/1.4750250.

[104] Kabashin A V., Meunier M. Synthesis of colloidal nanoparticles during femtosecond laser ablation of gold in water. J Appl Phys 2003;94:7941–3. doi:10.1063/1.1626793.

[105] Sylvestre JP, Kabashin A V., Sacher E, Meunier M. Femtosecond laser ablation of gold in water: Influence of the laser-produced plasma on the nanoparticle size distribution. Appl Phys A Mater Sci Process 2005;80:753–8. doi:10.1007/s00339-004-3081-4.

[106] Gamrad L, Rehbock C, Krawinkel J, Tumursukh B, Heisterkamp A, Barcikowski S. Charge balancing of model gold-nanoparticle-peptide conjugates controlled by the peptide's net charge and the ligand to nanoparticle ratio. J Phys Chem C 2014;118:10302–13. doi:10.1021/jp501489t.

[107] Marzun G, Nakamura J, Zhang X, Barcikowski S, Wagener P. Size control and supporting of palladium nanoparticles made by laser ablation in saline solution as a facile route to heterogeneous catalysts. Appl Surf Sci 2015;348:75–84. doi:10.1016/j.apsusc.2015.01.108.

[108] Mao SS, Mao X, Greif R, Russo RE. Initiation of an early-stage plasma during picosecond laser ablation of solids. Appl Phys Lett 2000;77:2464–6. doi:10.1063/1.1318239.

[109] Plech A, Kotaidis V, Lorenc M, Wulff M. Thermal dynamics in laser excited metal nanoparticles. Chem Phys Lett 2005;401:565–9. doi:10.1016/j.cplett.2004.11.072.

[110] Shih CY, Streubel R, Heberle J, Letzel A, Shugaev M V., Wu C, et al. Two mechanisms of nanoparticle generation in picosecond laser ablation in liquids: The origin of the bimodal size distribution. Nanoscale 2018;10:6900–10. doi:10.1039/c7nr08614h.

[111] Streubel R, Barcikowski S, Gökce B. Continuous multigram nanoparticle synthesis by high-power, high-repetition-rate ultrafast laser ablation in liquids. Opt Lett 2016;41:1486. doi:10.1364/ol.41.001486.

[112] Messina GC, Wagener P, Streubel R, De Giacomo A, Santagata A, Compagnini G, et al. Pulsed laser ablation of a continuously-fed wire in liquid flow for high-yield production of silver nanoparticles. Phys Chem Chem Phys 2013;15:3093–8. doi:10.1039/c2cp42626a.

[113] Barcikowski S, Meńndez-Manjón A, Chichkov B, Brikas M, Račiukaitis G. Generation of nanoparticle colloids by picosecond and femtosecond laser ablations in liquid flow. Appl Phys Lett 2007;91. doi:10.1063/1.2773937.

[114] Bärsch N, Jakobi J, Weiler S, Barcikowski S. Pure colloidal metal and ceramic nanoparticles from high-power picosecond laser ablation in water and acetone. Nanotechnology 2009;20. doi:10.1088/0957-4484/20/44/445603.

[115] Sajti CL, Sattari R, Chichkov B, Barcikowski S. Ablation efficiency of α-Al2O3 in liquid phase and ambient air by nanosecond laser irradiation. Appl Phys A Mater Sci Process 2010;100:203–6. doi:10.1007/s00339-010-5572-9.

[116] Schwenke A, Wagener P, Nolte S, Barcikowski S. Influence of processing time on nanoparticle generation during picosecond-pulsed fundamental and second harmonic laser ablation of metals in

tetrahydrofuran. Appl Phys A Mater Sci Process 2011;104:77–82. doi:10.1007/s00339-011-6398-9.

[117] Bärsch N. Improving Laser Ablation of Zirconia by Liquid Films: Multiple Influence of Liquids on Surface Machining and Nanoparticle Generation. J Laser Micro/Nanoengineering 2009;4:66–70. doi:10.2961/jlmn.2009.01.0013.

[118] Jiang Y, Liu P, Liang Y, Li HB, Yang GW. Promoting the yield of nanoparticles from laser ablation in liquid. Appl Phys A Mater Sci Process 2011;105:903–7. doi:10.1007/s00339-011-6557-z.

[119] Nguyen TTP, Tanabe-Yamagishi R, Ito Y. Impact of liquid layer thickness on the dynamics of nano- to sub-microsecond phenomena of nanosecond pulsed laser ablation in liquid. Appl Surf Sci 2019;470:250–8. doi:10.1016/j.apsusc.2018.10.160.